

# A tale of two tails and an off-centered envelope: diffuse light around the cD galaxy NGC 3311 in the Hydra I cluster<sup>★</sup>

Magda Arnaboldi<sup>1,2</sup>, Giulia Ventimiglia<sup>1,3</sup>, Enrica Iodice<sup>4</sup>, Ortwin Gerhard<sup>3</sup>, and Lodovico Coccato<sup>1,3</sup>

<sup>1</sup> European Southern Observatory, Karl-Schwarzschild-Str. 2, D-85748 Garching, Germany

<sup>2</sup> INAF, Osservatorio Astronomico di Pino Torinese, I-10025 Pino Torinese, Italy

<sup>3</sup> Max-Planck-Institut für Extraterrestrische Physik, Postfach 1312, Giessenbachstr., D-85741 Garching, Germany

<sup>4</sup> INAF, Osservatorio Astronomico di Capodimonte, I-80126 Napoli, Italy

Version May 12, 2012

## ABSTRACT

**Context.** The formation of intracluster light and of the extended halos around brightest cluster galaxies is closely related to morphological transformation, tidal stripping, and disruption of galaxies in clusters.

**Aims.** Here we look for observational evidence to characterize these processes, by studying the morphology and kinematics of the diffuse light in the core of the Hydra I cluster.

**Methods.** We analyze Ks- and V-band surface photometry as well as deep long-slit spectra, and establish a link between the structures in the light distribution, the absorption line kinematics, and the LOS velocity distributions of nearby galaxies and planetary nebulae (PNs).

**Results.** The central galaxy NGC 3311 is surrounded by an extended symmetric outer halo with  $n=10$  and an additional, off-centered envelope  $\sim R \sim 80''$  to the North-East. Its luminosity  $L_V = 1.2 \times 10^{10} (\pm 6.0 \times 10^8) L_\odot$  corresponds to  $\sim 50\%$  of the luminosity of the symmetric halo in the same region ( $\sim 15\%$  of its entire luminosity). The velocity dispersion of the halo rises to cluster core values,  $\sim 400 - 500 \text{ km s}^{-1}$ , for  $R > 20''$ . Based on measured PN velocities, at least part of the off-centered envelope consists of high-velocity accreted stars.

We have also discovered two tidal streams in the cluster center, emerging from the dwarf galaxy HCC 026 and from the S0 galaxy HCC 007. The HCC 026 stream is redshifted by  $\sim 1200 \text{ km s}^{-1}$  with respect to NGC 3311 ( $V_{N3311} \approx 3800 \text{ km s}^{-1}$ ), similarly as HCC 026 itself, a fraction of PNs in the off-centered envelope, and several other dwarf galaxies nearby. The stars in one of the HCC 026 tails are known to be consistent with the low-metallicity population of HCC 026, and our photometry shows that this galaxy is already mostly dissolved in the tidal field.

The tidal stream around HCC 007 extends over at least  $\sim 110 \text{ kpc}$ . It is fairly thick and is brighter on the side of the asymmetric outer halo of NGC 3311, which it may join. Its luminosity is several  $10^9 L_\odot$ , similar to the luminosity of the stripped-down galaxy HCC 007. The redshift of the stream is determined from a few PN velocities and is similar to that for HCC 007 and HCC 026.

**Conclusions.** An entire group of small galaxies is currently falling through the core of the Hydra I cluster and have already been partially dissolved by the strong tidal field. Their light is being added to the outer halo and intracluster light around the cD galaxy NGC 3311. The Hydra I cluster provides a vivid example of morphological transformation and tidal dissolution of galaxies in clusters.

**Key words.** galaxies:clusters:general – galaxies:clusters:individual (Hydra I) – galaxies:kinematics and dynamics – galaxies:individual (NGC 3311)

## 1. Introduction

Galaxy clusters are the most massive virialized structures in the universe, and may consist of thousands of galaxies. One of the most interesting fields in modern cosmology is the study of the mechanisms for the growth and evolution of such systems and the evolution of galaxies within them. The hierarchical model predicts that structure formation and evolution occurs through the merging of smaller units into larger systems, and this model has been supported by many observational evidences. The observational appearance of clusters and their galaxies additionally depends on the evolution of the baryonic component, which is less well understood. As galaxies fall into dense environments, their evolution is affected by a variety of dynamical processes

such as tidal interaction and harassment, mergers and cannibalism, gas stripping and starvation; see Poggianti (2004); De Lucia (2007) for reviews. Which of these mechanisms takes the leading role for a given galaxy morphological type in different environmental conditions still remains to be understood.

In the nearby universe, the evolution of clusters as a whole and the evolution of galaxies in clusters can be addressed by studying the dynamics of the intracluster light (ICL). The ICL is the diffuse light in galaxy clusters emitted by stars which are not bound to any specific galaxies; for a review on the subject see Arnaboldi & Gerhard (2010). Wide field surface photometry shows structures in the ICL on all scales, from a few arcminutes to degrees on the sky (Thuan & Kormendy 1977; Mihos et al. 2005; Rudick et al. 2009). Recent studies have shown that the ICL provides direct evidence for the dynamical status of galaxy cluster cores (Gerhard et al. 2007; Doherty et al. 2009; Ventimiglia et al. 2011), because it contains the fossil record of past interactions, due to its long dynamical time.

Send offprint requests to: M. Arnaboldi, e-mail: marnabol@eso.org

<sup>★</sup> Based on observations collected at the European Organization for Astronomical Research in the Southern Hemisphere, Chile, under the observing programs 082.A-0255(A), 076.B-0641(A), 065.N-0459

Cosmological hydro-dynamical simulations predict that the ICL is formed by stars that are unbound from galaxies during the interactions they experience as they fall through the cluster potential well and interact with other cluster galaxies and the cluster tidal field. In these simulations the ICL shows significant substructures on all scales in its spatial and velocity distribution (Napolitano et al. 2003; Murante et al. 2004; Willman et al. 2004; Sommer-Larsen et al. 2005). At early times the ICL morphology is dominated by long, linear features like streams that become more diffuse at later times as they spread in the cluster volume (Rudick et al. 2009). Most of the simulated intracluster stars become unbound from their parent galaxies during the merging history leading to the formation of the brightest cluster galaxy (BCG) in the cluster center, while for ICL at larger radii other mechanisms like tidal stripping are more important (Murante et al. 2007; Puchwein et al. 2010).

In this paper we report surface photometry and long slit spectroscopy of the ICL in the center of the Hydra I cluster, a medium compact cluster at  $\sim 50$  Mpc distance in the Southern hemisphere, with a central cD galaxy, NGC 3311. The aim is to compare the structures in the surface brightness distribution in the cluster core around NGC 3311 with kinematic information, including also the LOS velocities of intracluster planetary nebulae (ICPNs). Studying the kinematics of the ICL in nearby clusters like Hydra I is possible with ICPNs because (i) these objects are relatively easy to detect due to their strong  $[OIII]$  emission line (Jacoby 1989; Ciardullo et al. 1989), and (ii) they are good tracers of the light distribution of the parent stellar population (Buzzoni et al. 2006; Coccato et al. 2009). The LOS velocity distribution (LOSVD) of the ICPNs associated with the diffuse light in the central 100 kpc around NGC 3311 was determined by Ventimiglia et al. (2008, 2011). They found discrete velocity components at redshift  $\sim 1800 \text{ km s}^{-1}$  and  $\sim 5000 \text{ km s}^{-1}$ , in addition to a broad component with velocity dispersion  $\sigma \approx 500 \text{ km s}^{-1}$  approximately at the systemic velocity of the Hydra I cluster ( $\approx 3900 \text{ km s}^{-1}$ ). Ventimiglia et al. (2011) concluded that the broad velocity component in the ICPN LOSVD may trace the high-velocity dispersion outer halo of NGC 3311 (Ventimiglia et al. 2010), while the discrete components trace sub-components that fell through the cluster core, were tidally disrupted, and have not yet dynamically mixed in the gravitational potential.

This paper is structured as follows: in Section 2 we present optical V-band and 2MASS Ks-band images for the Hydra I cluster core. Isophote fitting and analysis of the surface brightness profiles is carried out in Section 3. Two-dimensional models for the NIR and optical data are derived in Section 4, showing the existence of an off-centered outer halo around NGC 3311 as well as tidal streams superposed on this halo. In Section 5, long slit spectroscopic data and kinematic measurements for the halo of NGC 3311 and the localized stream about HCC 026 are presented and discussed. In Section 6 we investigate the correspondence between the photometric components and kinematic substructures in the velocity distribution of Hydra I PNs, dwarf and S0 galaxies within 50 kpc of the center of NGC 3311. Section 7 briefly discusses the peculiar outer halo of NGC 3311, the properties of the newly discovered tidal streams, and the formation of ICL from this group of galaxies in disruption. Finally, Section 8 contains our summary and conclusions. We assume a distance to the Hydra I cluster of  $D = 50$  Mpc, so  $1'' = 0.247 \text{ kpc}$ .

## 2. Optical and Near Infrared imaging of the Hydra I cluster core

The core of the Hydra I cluster is dominated by two giant elliptical galaxies, NGC 3311 and NGC 3309. Early CCD surface photometry showed that both NGC 3311 and NGC 3309 are fitted by an  $R^{1/4}$  law within  $30''$  distance from their centers (Vasterberg et al. 1991). On the basis of the large  $R_e = 98''$  value from the  $R^{1/4}$  fit, Vasterberg et al. (1991) classified NGC 3311 as a cD galaxy. In the center of this galaxy, a complex dust lane is found, and the observed surface brightness profile thus falls below the best fit  $R^{1/4}$  profile. Both the dust lane and the core in the central profile are confirmed by HST WFPC2 imaging (Laine et al. 2003). NGC 3309 does not have a dust lane in its core (Vasterberg et al. 1991). Misgeld et al. (2008) published VLT/FORS1 images of the Hydra cluster in the V-band, that were used by Richtler et al. (2011) to derive the average radial surface brightness profile for NGC 3311 down to  $\mu_V = 26.5 \text{ mag arcsec}^{-2}$ . They classified NGC 3311 as a cD galaxy because of the low central surface brightness and extended radial profile.

In the present work we derive accurate quantitative photometry for the galaxy NGC 3311, NGC 3309 and the diffuse light in the Hydra I core. In what follows, we use three data sets for this purpose: 2MASS Ks band data, VLT/FORS1 archive data for the center of the Hydra I cluster, and V band images obtained with WFI at the ESO/MPI 2.2m telescope. Because of the absorption caused by the central dust lane and its effect in the optical bands, near infrared (NIR) photometry is required for an accurate study of the central light distribution. The V band images allow us to measure the profile shape at large radii where the surface brightness is low, and analyze the substructures in the light distribution. The VLT/FORS1 and 2.2m/WFI data contain complementary information: the FORS1 data are deep, and allow reliable measurements down to  $\mu_V = 26.5 \text{ mag arcsec}^{-2}$  (Richtler et al. 2011), while the WFI data with their large field-of-view provide a robust estimate of the sky background.

### 2.1. Ks-band photometry - 2MASS archive data

We retrieved a  $9' \times 7'$  Ks-band image with a pixel scale of  $1'' \text{ pixel}^{-1}$ , centered on the galaxy NGC 3311 in the core of the Hydra I cluster, from the 2MASS archive (<http://irsa.ipac.caltech.edu/cgi-bin/2MASS/LGA/>). This image includes both NGC 3311 and NGC 3309. The 2MASS archive images are already reduced and flux calibrated, with a zero point for the Ks-band photometry  $ZP_{Ks} = 19.91$  with 2-3% uncertainty (Jarrett et al. 2003).

In this image, we can reliably measure surface brightness values down to  $19 \text{ mag arcsec}^{-2}$  in the Ks-band, corresponding to a distance of  $\sim 45''$  from the center of NGC 3311. We use the K-band image as reference to characterize the shape of the surface brightness profile for the bright regions and limit the influence of the dust lane on the structural parameters, see Sect. 3 and 4.1.

### 2.2. VLT/FORS1 deep V band photometry - Observations and data reduction

Johnson V band imaging data for NGC 3311 and NGC 3309 were retrieved from the ESO Science Archive Facility, acquired with VLT/FORS1 in service mode on April 04, 2000 (program 65.N-0459(A), PI Hilker). The VLT/FORS1 images cover a field-of-view (FoV) of  $6.8' \times 6.8'$  at an angular scale of  $0''.2 \text{ pixel}^{-1}$ . During the observations, the FoV was centered at  $\alpha =$

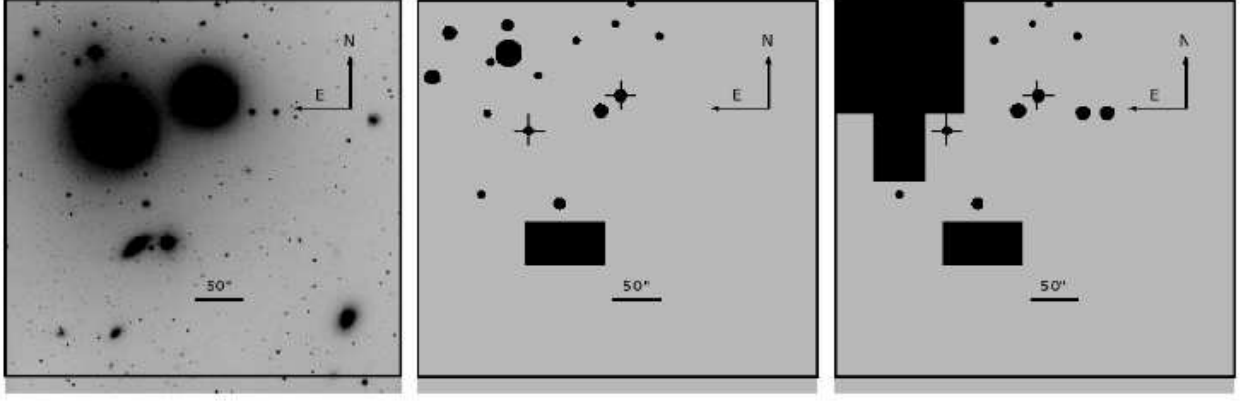


**Fig. 1.** Left panel - VLT/FORS1 V band co-added image of the Hydra I cluster core with NGC 3311 and NGC 3309 visible in the upper part of the image. A 2D-photometric model is fit within the region of  $6'.8 \times 6'.4$  limited by the box (see Sect. 4.2 for details). Middle panel - The mask “cmask” adopted for the 2D-model fit of the VLT/FORS1 data, which masks stars and galaxies in the chosen region as well as the centers of NGC 3311 and NGC 3309. Right panel - The mask “allmask” for the 2D fit that masks also part of the North-East regions in addition to the stars and galaxies in “cmask” (see Sect. 4.1 and 4.2 for details). In the middle and right panels, the two crosses indicate the positions of the centers of the two giant galaxies.

10h36m36.14s,  $\delta = -27^{\circ}32'51''$ , avoiding a bright star NE of NGC 3311. The dataset included three exposures of 480 sec each for a total observing time of 0.4 hr. The resulting average seeing in the combined median image is  $FWHM \sim 0''.6$ ; the central  $\sim 5''$  diameter region of NGC 3311 and  $\sim 8''$  diameter region of NGC 3309 are saturated.

Standard calibrations, bias, and sky flats were also retrieved from the ESO Archive. Several Landolt standard stars in the Rubin 152 field were observed in V band for the photometric calibration. The zero point for the V band VLT/FORS1 photometry  $ZP_{V,FORS1} = 27.43 \pm 0.06$  is derived independently in the present work. The correction for extinction in the V band amounts to 0.25 mags (Schlegel et al. 1998).

The instrumental signature of the VLT/FORS1 images was removed using standard IRAF tasks. Spikes from saturated stars in the field were also removed; see Section 2.3. Images were registered before co-addition; the co-added final VLT/FORS1 V band image is shown in Fig. 1.

### 2.3. Wide Field Imager V band photometry - Observations and data reduction

Johnson V band imaging of the Hydra I cluster was acquired in service mode on the night of January 12, 2006 at the Wide Field Imager (WFI) on the ESO/MPI 2.2m telescope, at the La Silla observatory. The WFI imager covers a field-of-view (FoV) of  $34' \times 33'$  with a mosaic of  $4 \times 2$  CCDs ( $2k \times 4k$ ) at an angular scale of  $0''.238 \text{ pixel}^{-1}$ . During the observations, the FoV was centered at  $\alpha = 10^{\text{h}}36^{\text{m}}51^{\text{s}}$ ,  $\delta = -27^{\circ}31'35''$ . 13 exposures of 300 sec each were obtained for a total observing time of  $\sim 1.1$  hr. The resulting average seeing in the combined median image is  $FWHM \sim 0''.7$ .

Standard calibrations, bias, sky flats and dark skies, were also obtained. Several Landolt standard stars in the Rubin 149 field were observed in V band for the photometric calibration. The zero point for the V band photometry is  $ZP_V = 24.02 \pm 0.02$ .

Data reduction is carried out with standard IRAF tasks for pre-reduction and calibration. After bias subtraction and flat fielding, the frames are corrected for any residuals by using dark skies. Then the average background emission is measured in several regions of the FoV far from the galaxy light and the final av-

erage value is subtracted off each single frame. The IRAF task *NOAO.NPROTO.IRMOSAIC* is used to obtain a mosaic of the CCDs. Each frame is inspected and bright spikes associated with saturated stars are removed by linear interpolation from nearby columns/rows before frames are co-added. Residual sky offsets with respect to the average value are removed before the CCD frames are mosaiced. Finally, the mosaic images are registered. Then image fluxes are scaled to a reference image to account for transparency variations, following which images are co-added with a threshold rejection implemented to reduce effect from CCD gaps. The final co-added image is shown in the left panel of Fig. 2.

As a first step in the study of the light distribution in NGC 3311, we determine the extension of the dust lane in its central region. We use the *FMEDIAN* task in IRAF with a smoothing box of  $15 \times 15$  pixels, and compute the ratio of the V band image and its *FMEDIAN* smoothed version; the resulting unsharp masked V-band image is shown in Figure 3.

This figure illustrates the presence of several distinct components at the center of NGC 3311. A complex dust lane crosses the galaxy center in the direction North-South (NS) and extends to about  $3''$  in radius, see the high angular resolution image in Laine et al. (2003). Bright knots are seen East and Southwest of the galaxy center, within and around the dust lane out to  $8''$  in radius. According to Vasterberg et al. (1991), the dominant knot is bluer,  $\Delta(B-r) = -0.10$ , than the surrounding stellar population.

## 3. Surface photometry for NGC 3311 in V and Ks band

In this Section, we describe isophotal analysis for the light distribution of NGC 3311, both from the V-band and 2MASS Ks-band data. We then derive V-band surface brightness profiles along several specific directions through the galaxy to characterize the deviations from a simple concentric elliptical light distribution.

### 3.1. Isophote fitting

We use the *ELLIPSE* task in IRAF on the Ks and V images to perform the isophotal analysis of NGC 3311. Position an-

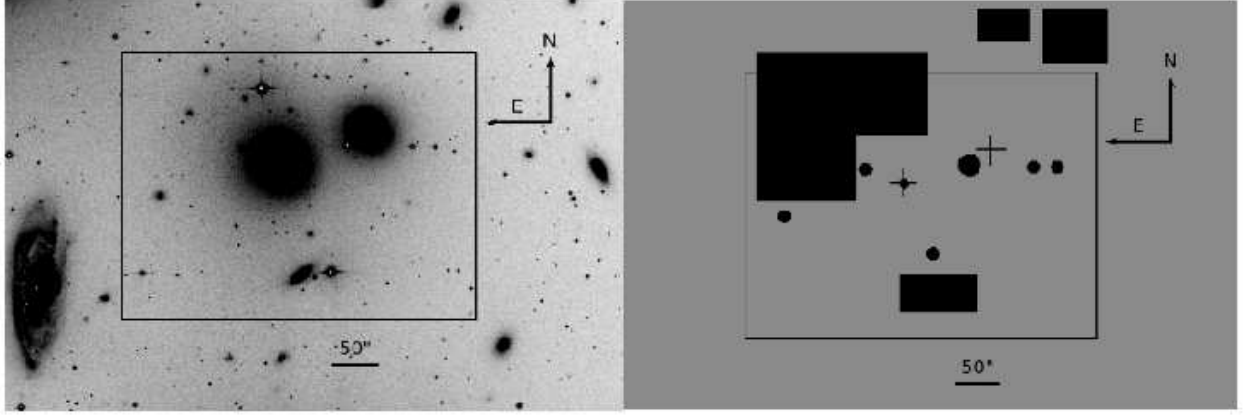


**Fig. 2.** Left panel - 2.2m/WFI V band image of the Hydra I cluster core; NGC 3311 is visible on the left and NGC 3309 on the right. A 2D-photometric model is fit within the region of  $6'.4 \times 4'.8$  limited by the box. Right panel - The mask “allmask” adopted for the fit to the bright central regions (see Sect. 4.3 for details). The two crosses in the right panel indicate the positions of the centers of NGC 3311 and NGC 3309.

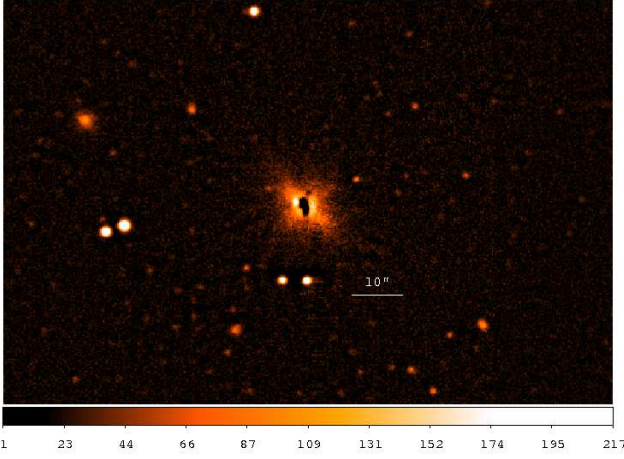


**Fig. 3.** Unsharp masked V band image obtained from optical data acquired at the ESO/MPI 2.2m telescope with the WFI; North is up, and East to the left. The white bar indicates  $10''$  length. The inner dust lane at the center of NGC 3311 is about  $2''$  wide and  $7''$  long (Laine et al. 2003), and is embedded within a central light excess of about  $16''$  in diameter, where bright knots are visible here and in the HST image of Laine et al. (2003).

gle (P.A.), ellipticity, and average surface brightness profiles for NGC 3311 are shown in Figure 4.

The *ELLIPSE* V-band average surface brightness profile extends out to  $80''$  from the galaxy center before the halo light from NGC 3309 becomes significant. Note the excellent agreement between the VLT/FORS1 and WFI surface brightness profiles. The Ks-band profile is less extended and reaches  $\sim 60''$  (see also Sect. 2.1). The total integrated magnitudes inside circular apertures, whose radius corresponds to the last measured point, are:  $m_V^{WFI}(R = 77''.4) = 11.55$  mag;  $m_V^{FORS}(R = 71''.5) = 11.36$  mag;  $m_K(R = 61''.9) = 8.41$  mag. The half-light radii evaluated from the light-growth curves out to the last measured point are  $R_{g,V}^{WFI} = 36'' \pm 2''$  ( $\sim 8.9$  kpc),  $R_{g,V}^{FORS} = 32'' \pm 2''$  ( $\sim 7.9$  kpc),  $R_{g,K} = 33'' \pm 3''$  ( $\sim 8.1$  kpc).

At  $R \leq 5''$ , the presence of a dust-lane is signaled by the large variations in the V-band ellipticity and P.A. profiles. Between  $5''$  and  $15''$  the V-band isophotes twist by about 20 degrees: this is

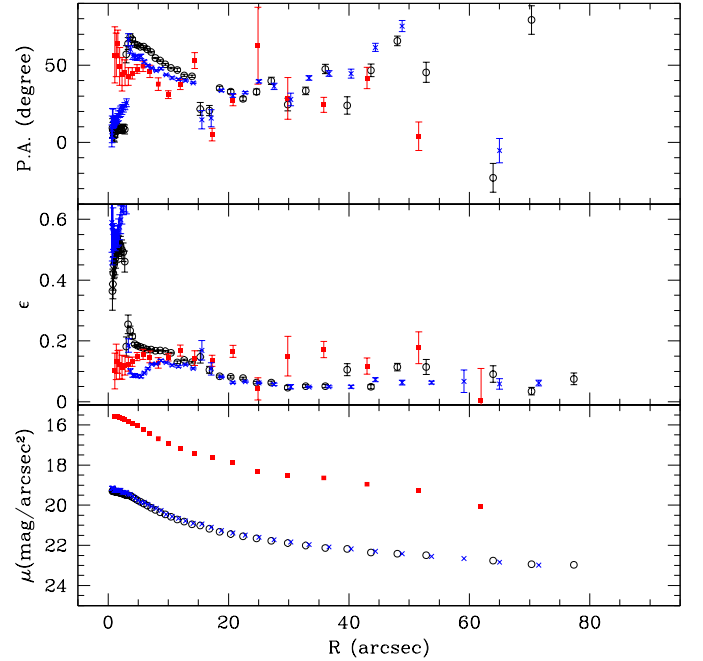


**Fig. 4.** One dimensional profiles of the P.A. for the isophote major axis, ellipticity, and surface brightness obtained with *ELLIPSE* from Ks-band (red full dots) and V-band images of NGC 3311 (VLT/FORS1 blue crosses, 2.2m/WFI black open dots).

caused by the presence of the inner bright knots seen around the dust lane (see Sect. 2.3). A twist of the NGC 3311 isophotes is also reported by Vasterberg et al. (1991), but the P.A. variation was not quantified. For radii  $15'' < R < 45''$ , the V-band ellipticity and P.A. profiles are nearly constant, with average values  $\epsilon \simeq 0.05$  and  $P.A. \simeq 32^\circ$ , i.e., the isophotes in this region are nearly round.

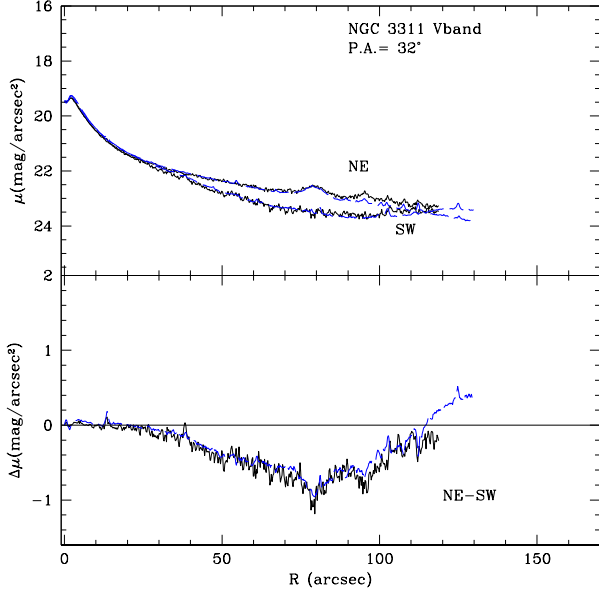


**Fig. 5.** Upper panel: folded V-band profiles extracted along P.A.= 32° (major axis, 2.2m/WFI black full lines, VLT/FORS1 blue dashed lines). NE is along P.A.= 32° and SW along P.A.= 212°. Lower panel: difference profiles. The folded profile along the major axis illustrates the excess of light in the NE quadrant of the NGC 3311 halo, in the range of radii  $20'' < R < 120''$ , with a maximum excess of about one magnitude at  $R = 80''$ .

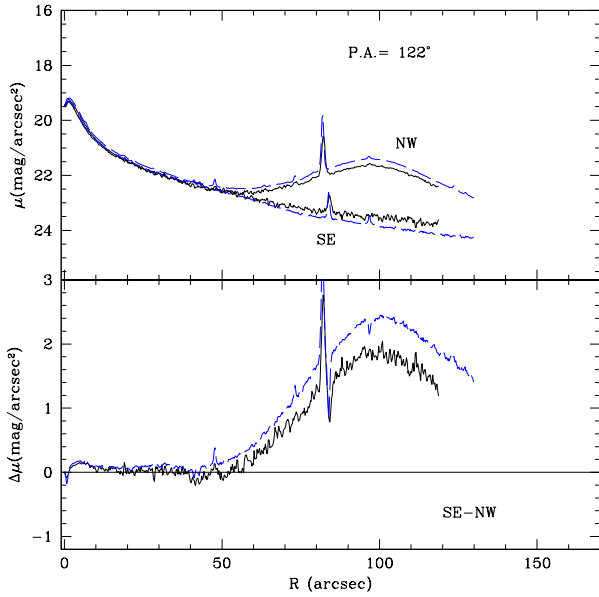


**Fig. 6.** Same as Fig.5. Upper panel: folded V-band profiles extracted along P.A.= 122° (minor axis, 2.2m/WFI black full lines, VLT/FORS1 blue dashed lines). SE is along P.A.= 122°, NW along P.A.= 302°. Lower panel: difference profiles. On the NW side, for  $R \geq 65''$  we see the contribution from the outer regions of NGC 3309.

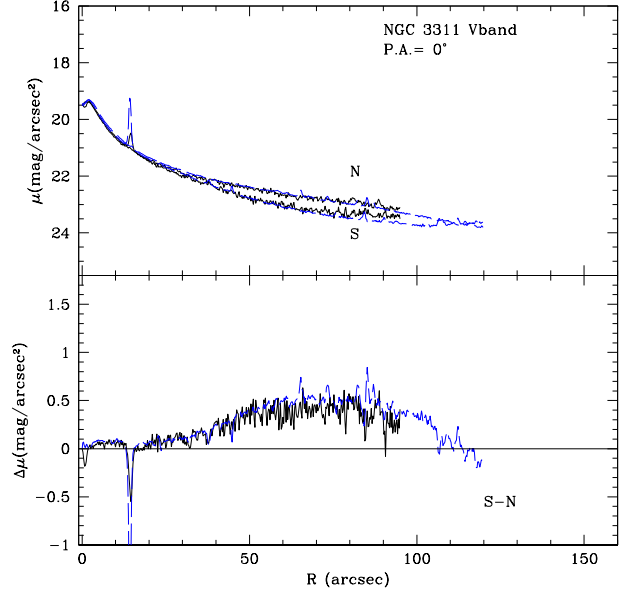


**Fig. 7.** Same as Fig.5. Upper panel: folded V-band profiles extracted along P.A.= 0° (2.2m/WFI black full lines, VLT/FORS1 blue dashed lines). N is along P.A.= 0°, S along P.A.= 180°. Lower panel: difference profiles.

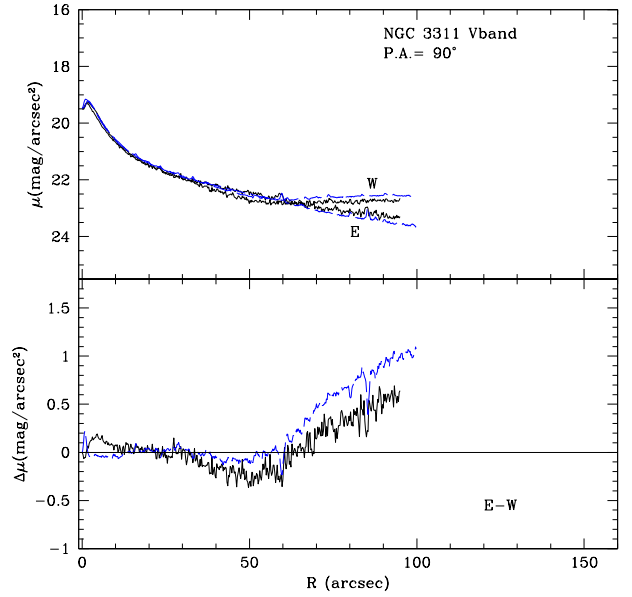


**Fig. 8.** Same as Fig.5. Upper panel: folded V-band profiles extracted along P.A.= 90° (2.2m/WFI black full lines, VLT/FORS1 blue dashed lines). E is along P.A.= 90°, W along P.A.= 270°. Lower panel: difference profiles.

### 3.2. Analysis of surface brightness profiles along principal axes of the light distribution

The position angle profile from the isophote fit in Fig. 4 has a complicated radial dependence which we show now is related to asymmetries in the light distribution. To this end we investigate separately the surface brightness profiles along several axes across the light distribution in NGC 3311. From the isophote

fitting, the major axis is at P.A. =  $32^\circ$  and the minor axis is at P.A. =  $122^\circ$ . Along these directions, we have extracted one-dimensional (1D) surface brightness profiles from the Ks band, V-band VLT/FORS1 and 2.2m/WFI images.

While the Ks band profiles show an azimuthally symmetric light distribution (Sect. 4), the V band surface brightness profiles become asymmetric for  $R > 30''$ , as shown in Figs. 5 and 6. The major-axis profile at P.A. =  $32^\circ$  (North East - NE) is up to one magnitude brighter than that at P.A. =  $212^\circ$  (South-West - SW) in the radial range  $20'' < R < 120''$  (Fig. 5). There is additional light along P.A. =  $212^\circ$  at  $R \geq 100''$  which may be related with a substructure in the Hydra I core. This will be further investigated in the residual image, once the light distribution from the bright galaxies is accounted for. The light profiles along the minor axis, at P.A. =  $122^\circ$  (South East - SE) and P.A. =  $302^\circ$  (North West - NW) are symmetric for  $R < 60''$  (Fig. 6). At P.A. =  $302^\circ$  and  $R > 60''$  we see the light from the NGC 3309 halo. For  $R \leq 5''$ , both V band profiles show the absorption by the central dust-lane.

In addition, we extract folded profiles along the NS (P.A. =  $0^\circ$ ) and EW (P.A. =  $90^\circ$ ) directions. These are also asymmetric; see Fig. 7 and Fig. 8. At P.A. =  $0^\circ$  and  $R \geq 20''$ , the galaxy becomes brighter than at P.A. =  $180^\circ$ ; the difference is about 0.5 mag at  $R = 80''$  (Fig. 7). At P.A. =  $90^\circ, 270^\circ$  the profiles are symmetric for  $R \leq 30''$ , while in the radial range  $30'' \leq R \leq 60''$  the profile at P.A. =  $90^\circ$  is brighter (by about 0.2 mag at  $R \sim 50''$ ) than that at P.A. =  $270^\circ$ . At larger radii the profile is affected by the light of NGC 3309.

The VLT/FORS1 and 2.2m/WFI profiles in Figs. 5 and 7 show very good agreement on both the N/NE and S/SW sides of NGC 3311 and also in the difference profiles. This shows that systematic effects caused by scattered light from the bright star NE of NGC 3311 are negligible and that there are no residual gradients due to the sky background along these directions. Figs. 6 and 8 show a small relative variation between the W/NW and E/SE sides, amounting to  $\sim 0.2$  mag over  $100''$ . This may be due to a residual gradient in the background of one of the images. As we will discuss further in Sect. 4.3, this does not affect our main results.

The analysis presented in this Section illustrates that the halo of NGC 3311 is asymmetric. Between P.A. =  $0^\circ$  and P.A. =  $90^\circ$ , and in the radial range  $30'' < R < 120''$ , it is brighter than in the remaining three quadrants.

#### 4. Models for the light distribution in NGC 3311, NGC 3309, and the residual diffuse light in the Hydra I cluster core

In this Section we construct two dimensional (2D) surface brightness models for the light distribution in the Hydra cluster core around NGC 3311. Any such model must include the light distribution of NGC 3309, because the outer regions of the two elliptical galaxies overlap along the LOS. Furthermore, the modeling must also account for the asymmetric bright component in the NE outer region of NGC 3311, signaled by the asymmetry of the extracted profiles in Section 3.2. We adopt a staged approach, where we first study the inner symmetric parts in the Ks band, and then address the low surface brightness structures at large radii in the V-band.

##### 4.1. Ks-band 2D model for NGC 3311 and NGC 3309

We begin by constructing a 2D model of the light distribution in the Ks-band, using the GALFIT program of Peng et al. (2002). On the basis of the morphological classification available in NED (NGC 3311 cD2, and NGC 3309 E3), the light of both galaxies is fit using single Sersic laws (Sersic 1968). Because of the complex inner structure, the central region ( $R < 5''$ ; see Fig. 3) of NGC 3311 is masked in the fit. The 2D model and the residual images are shown in Fig. 9 and, with the exception of the galaxy centers, no significant residual structures are visible around either NGC 3311 or NGC 3309.

The results of the modeling show that the light distribution of NGC 3309 is reproduced by a Sersic profile with  $n_K \sim 2$ ; the most important GALFIT parameters for this galaxy are given in Table 1. For NGC 3311, a de Vaucouleurs law gives a good fit to the Ks light distribution; the corresponding GALFIT parameters are listed in Table 2. In the radial range  $5'' < R < 30''$  residuals are less than 0.2 mag, see Fig. 10. We conclude that a de Vaucouleurs model with  $b/a = 0.89$  and P.A. =  $36^\circ$  is an accurate model for the 2D Ks band surface brightness distribution of NGC 3311 in this radial range.

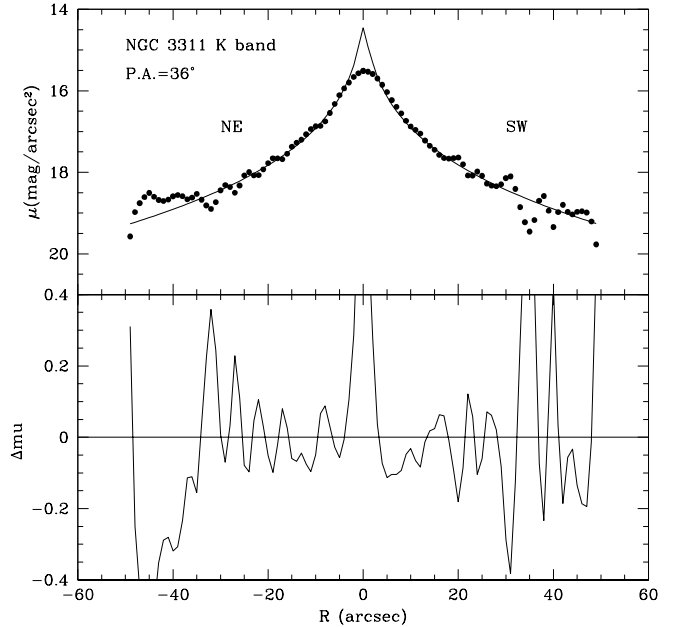


**Fig. 10.** 2D GALFIT model in the Ks band for NGC 3311 compared to major axis photometry. Upper panel: observed (black points) and fitted (black line) light profiles, extracted along the major axis of NGC 3311. Bottom panel: residual major axis profile obtained as “observed - 2D model” surface brightness.

##### 4.2. V-band 2D model for NGC 3311 and NGC 3309

Next we model the surface brightness distribution of NGC 3311 and NGC 3309 from the V band VLT/FORS1 image. For fitting the model to the VLT/FORS1 data, we first adopt the mask shown in the middle panel of Fig. 1, identified as “cmask” in what follows. It masks the saturated/bright stars in the field, the central  $R < 5''$  of NGC 3311, a region  $R < 8''$  around the saturated center of NGC 3309, and the background galaxies.



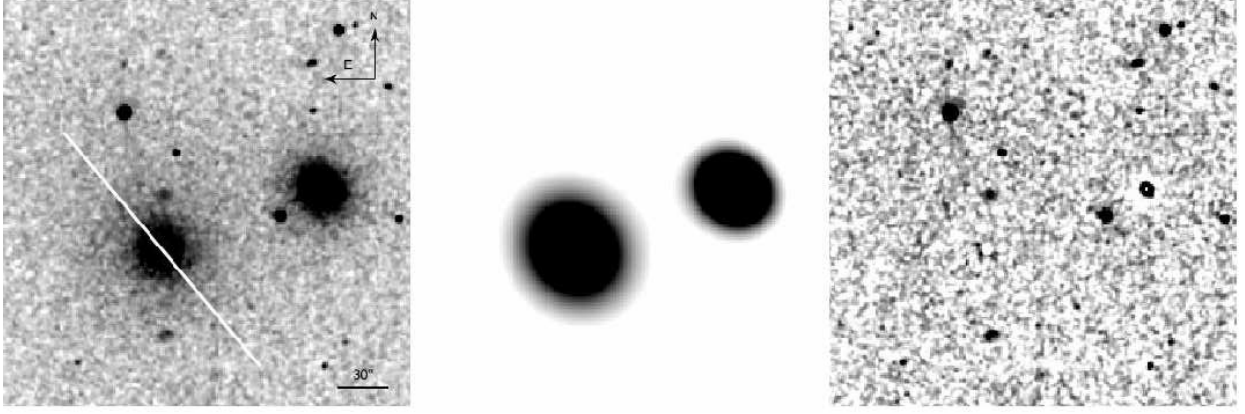


**Fig. 9.** Left panel: Ks band image of the Hydra I cluster core; the size of the image is  $3'.0 \times 2'.8$ . The two main galaxies are NGC 3311 (center) and NGC 3309 (right). The white line indicates the direction of the extracted light profiles in Fig. 10. Central panel: 2D model for the Ks surface brightness distribution of NGC 3311 and NGC 3309 obtained with GALFIT. Right panel: residual image obtained as the difference between the Ks-band image and the GALFIT model. North is up and East to the left. Darker colors are for brighter regions.

For the “cmask” model fit, the 2D Sersic model has parameters  $n_V = 3.3$ ,  $R_e = 21''.1$  for NGC 3309 and  $n_V = 5.0$ ,  $R_e = 270''.6$  for NGC 3311; see Tables 1 and 2. The residual V band image has more structures than in the Ks-band. In particular, to the SW of NGC 3311 around the galaxy’s major axis at P.A. =  $212^\circ$ , in a  $\sim 90^\circ$ -wide cone and radial range  $40'' < R < 80''$ , we see (unphysical) negative residuals of about 260 ADU per pixel with respect to the sky counts measured in the “empty” eastern boundary of the VLT/FORS1 image. This negative residual signals that NGC 3311 is fainter than the 2D Sersic model there. The region of negative residual derives from fitting an azimuthally averaged model to an intrinsically asymmetric galaxy; we saw previously in Sect. 3.2 that the galaxy is brighter in the NE quadrant than in the other three quadrants.

Therefore, we next investigate whether by masking the whole North-East quadrant of NGC 3311, the “symmetric” 2D model for the V band light in NGC 3311 will acquire a lower value for the Sersic index  $n$ , and thus the problem of negative residuals at P.A. =  $212^\circ$  is reduced. We define a new mask which additionally covers most of the NE quadrant in the NGC 3311 halo: this is shown in the right panel of Fig. 1 and is identified as “allmask”. When the light excess is masked, the GALFIT 2D fit to the V band FORS1 image returns a Sersic index  $n_V = 4.8$  and  $R_e = 198''.8$  for NGC 3311. The GALFIT model of NGC 3309 and NGC 3311, using “allmask” with the VLT/FORS1 data, and the residual image (difference between image and model) are shown in Figure 11. Parameters are given in Tables 1 and 2.

The residual image still shows negative values in the same region in a  $\sim 90^\circ$ -wide cone around P.A. =  $212^\circ$  and for the radial range  $40'' < R < 80''$ , but the level is now reduced to 110 ADU per pixel, compared to 260 ADU per pixel in the “cmask” residual image. Therefore the extra light in the NE of NGC 3311 must extend slightly further than the masked area. In addition, the residual image shows several positive structures which correspond to additional light in the real image with respect to the 2D models of NGC 3311 and NGC 3309, at a level of 200-500 ADU per pixel relative to sky. The morphologies of these luminous structures are consistent in both the “cmask” and “allmask” residual images, and they are brighter in the latter image. They are described here below:

- In the outer regions, NGC 3311 is more luminous than the best fit 2D model in a wide area covering the whole NE quadrant to the galaxy. Superposed on this envelope we also see a prominent tidal stream around HCC 026, one of the dwarf galaxies in the Hydra I cluster core. The stream is outlined by the red dashed lines in Fig. 11 at  $\sim 43''$  distance from the NGC 3311 center. The tidal tails around HCC 026 extend about 15 kpc NW and 5 kpc NE of the dwarf galaxy.
- The S0 galaxy HCC 007 situated  $119''$  South of NGC 3311 appears to be embedded in an extended, thick, tidal stream visible at faint surface brightness levels. Emerging from HCC 007, the stream circles the south part of the Hydra I core, it encompasses both NGC 3311 and NGC 3309, and extends over at least  $450''$  ( $\sim 110$  kpc), as indicated by the dashed blue lines in Fig. 11. The eastern tail of HCC 007 appears to join the bright envelope to the NE of NGC 3311; as part of the envelope it may continue considerably further to the north.
- In the center, at  $5'' < R < 10''$  and along the NE direction, NGC 3311 is more luminous than the 2D Sersic  $n_V = 4.8$  model. The extra light corresponds to the bright knots seen in the unsharp-masked 2.2m/WFI V-band image in Fig. 3.
- For NGC 3309, the residual image shows a brighter, N-S-oriented structure around the central masked area, possibly indicating that the isophotes are more circular at larger radii than in the inner parts. The positive residual structures at large radii around NGC 3309 are part of the extended tidal tail around HCC 007.

Fig. 12 shows 1D surface brightness profiles extracted along the NE and SW sides of the major axis of NGC 3311, as illustrated in Fig. 11. For radii  $5'' < R < 30''$ , the extracted profiles are straight lines in the  $R^{1/4}$  plot, consistent with the 2D GALFIT model for the Ks band data. Deviations from a de Vaucouleurs profile become large at  $R > 30''$  on the NE side (P.A. =  $32^\circ$ ), indicating additional light there. This additional light is composed of a large scale component that dominates the profile from  $30''$  to  $120''$ , and a bright substructure with  $\mu_{V,max} \simeq 22.5$  mag arcsec $^{-2}$ ,  $15''$  wide, at  $R \simeq 43''$ . This radially confined substructure is caused by the tidal stream emerging from the dwarf

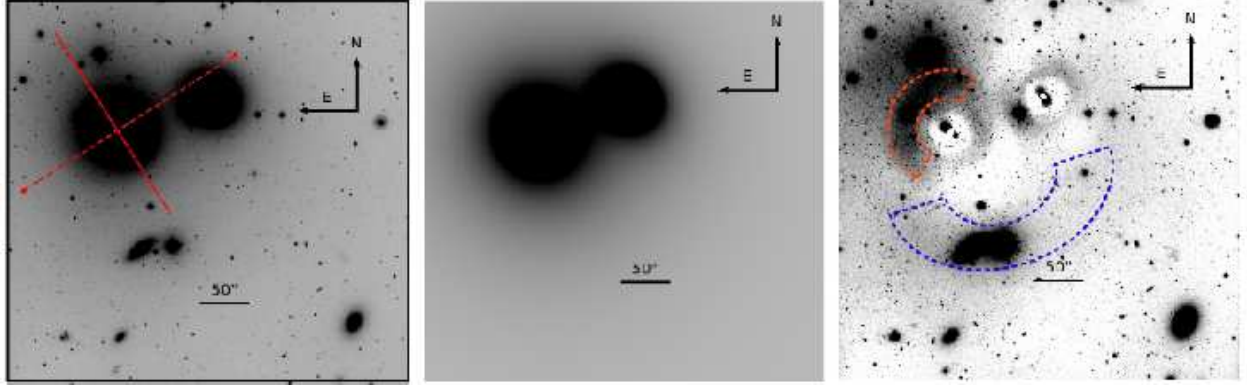


**Fig. 11.** GALFIT model of the VLT/FORS1 image obtained with “allmask” (see right panel of Fig. 1). Left panel: VLT/FORS1 V band image. Full and dashed red lines indicate the major axis at PA=32°, and the minor axis, respectively. Center panel: GALFIT 2D model for NGC 3311 and NGC 3309. Right panel: residual image. The red dashed curves outline the tidal stream around HCC 026, which is superposed on a brighter region NE of NGC 3311. The blue dashed lines outline the faint, thick stream around the S0 galaxy HCC 007 South of NGC 3311. The image size in all panels is 6'.8 × 6'.4, and darker colors indicate brighter regions.

Parameter	Ks-band	V band FORS1	V band FORS1	V band FORS1 min. symmetr.
Comp. type	Sersic	Sersic	Sersic	Sersic
$m_{tot}$	8.6 ± 0.01	11.6 ± 0.05	11.6 ± 0.05	11.2 ± 0.01
$R_e$	13''.1 ± 0''.10	21''.1 ± 0''.07	21''.9 ± 0.07	35'' ± 0.25''
$n$	2.2 ± 0.01	3.3 ± 0.02	3.3 ± 0.02	5.7 ± 0.04
b/a	0.87 ± 0.01	0.87 ± 0.01	0.85 ± 0.01	0.87 ± 0.01
P.A.	49.7 ± 0.9	48.2 ± 0.2	50.7 ± 0.2	49.8 ± 0.2
mask	none	“cmask”	“allmask”	“allmask”

**Table 1.** Parameters for the 2D GALFIT models of NGC 3309. Apparent V band total magnitudes are in agreement with the published NED values (RC3).

Parameter	Ks-band	V band FORS1	V band FORS1	V band FORS1 min. symmetr.
Comp. type	De Vauc.	Sersic	Sersic	Sersic
$m_{tot}^*$	7.4 ± 0.01	9.7 ± 0.01	10.1 ± 0.01	9.52
$R_e$	90'' ± 1	270''.6 ± 3''.4	198''.8 ± 2''.2	850'' ± 50''
$n$	4.0	5.0 ± 0.02	4.8 ± 0.02	10.5 ± 0.1
b/a	0.89 ± 0.01	0.93	0.93	0.93
P.A.	36 ± 1	38 ± 0.5	32	32
mask	none	“cmask”	“allmask”	“allmask”

**Table 2.** Parameters for the 2D GALFIT fit models of NGC 3311.

\* The  $m_{tot}$  and  $R_e$  values computed from the GALFIT fit model for NGC 3311 are respectively brighter and larger than those computed in Sect. 3.1 from the V band light growth curve, because the latter is measured only out to 71''.5, while the 2D model is fit to the whole 6'.8 × 6'.4 area.

galaxy HCC 026, which is seen in projection onto the NE bright envelope (see the red dashed lines in Fig. 11).

The flattening of the surface brightness profile at P.A.= 32° in Fig. 12 with respect to the steeper profile at P.A.= 212° indicates that at radii larger than 30'', the outer surface brightness contours shift towards the NE; i.e., the envelope is off-centered to the NE relative to the bright central region of NGC 3311. This confirms the asymmetries of the extracted surface brightness profiles discussed in Sect. 3.

Fig. 12 also explains the origin of the negative residuals in the “allmask” model: the surface brightness profile fitted by GALFIT (red full line) falls slightly above the SW (P.A.= 212°) major axis profile because of the surface brightness drop around 30 arcsec, so that the symmetric 2D model built from this pro-

file generates negative values in the residual image about P.A.= 212°.

In the next Section, we will improve on this by constructing a “minimal” symmetric model for the light centered on NGC 3311. Then we will use this to construct a new 2D model, and to discuss the structures in the corresponding residual image in more detail.

#### 4.3. The asymmetric light distribution around NGC 3311: extended off-centered envelope and tidal tails

We build a minimal symmetric model (MSM) for NGC 3311 in two steps. First, we fit the steep surface brightness profile towards SW, along P.A.= 212°, with a Sersic law. Fig. 12 shows



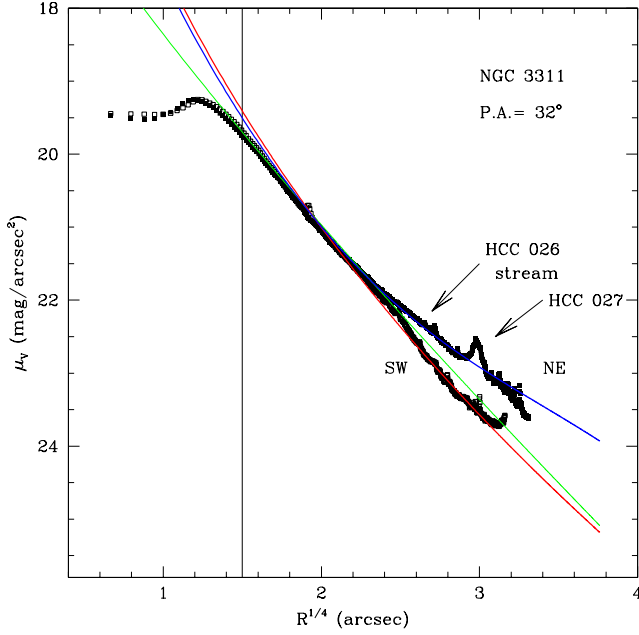


**Fig. 12.** Folded 1D surface brightness profile along the major axis of NGC 3311 plotted as function of  $R^{1/4}$ . Open symbols show values along P.A. = 212° (SW), full symbols those along P.A. = 32° (NE of the galaxy center). The green continuous line shows the extracted 1D major axis profile of the Sersic “allmask” model for the V-band FORS1 data described in Sect. 4.2. The red continuum line is the major axis profile for the light centered on NGC 3311 (“minimal” symmetric model, MSM). The blue full line shows the 1D fit to the surface brightness profile along P.A. = 32° (NE) with a two component model, consisting of the ‘MSM plus a one-sided exponential profile’. The two arrows indicate the position of the stream around HCC 026 and the light at  $R \approx 80''$  associated with the dwarf galaxy HCC 027. See Sect. 4.3 for details.

this profile over-plotted on the data (red line); the model fits the data well in the radial range 15''–80''. The parameters are  $n_V = 10.5 \pm 0.1$ ,  $R_e = 850'' \pm 50''$ , and  $\mu_e = 28.07 \pm 0.1$  mag arcsec $^{-2}$ ; see Table 2.

To quantify the asymmetry in the NGC 3311 halo, we also fit the NE surface brightness profile (P.A. = 32°) with a two-component model, consisting of a Sersic law with the same  $n$  and  $R_e$  and an additional exponential profile for the outer regions. The exponential profile often is a good approximation for the outer stellar envelopes of cD galaxies (Seigar et al. 2007). This combined model provides a good fit to the NE profile which is also shown in Fig. 12 (blue line); the parameters are  $n_V = 10.5 \pm 0.1$ ,  $R_e = 850'' \pm 50''$  and  $\mu_e = 28.2 \pm 0.1$  mag arcsec $^{-2}$  for the Sersic component, and  $\mu_0 = 23.2 \pm 0.1$  mag arcsec $^{-2}$  and  $r_h = 200'' \pm 50''$  for the exponential component.

As a second step, we use GALFIT with the mask “allmask” to generate a 2D MSM for NGC 3311, using the Sersic law with parameters set from the 1D best fit, and the major axis PA=32° and axis ratio 0.93 from our previous 2D model fits. Then, keeping this component fixed, we use GALFIT again to determine new best fit parameters for NGC 3309, matching a Sersic model to the remaining light. Results of this NGC 3309 fit are listed in Table 1. Adding both components, we obtain the MSM for the

two bright galaxies NGC 3311 and NGC 3309. By construction, the residual image obtained as the difference between the V-band VLT/FORS1 image and this MSM should show only positive or null residual values around NGC 3311 (outside the central  $R < 15''$  containing dust and bright knots).

This residual image, displayed in Fig. 13, clearly shows the presence of an additional, extended envelope, off-centered towards the NE of the inner regions of NGC 3311. It is highlighted by the white dashed ellipse in Fig. 13. The residual image also shows the bright tail around HCC 026, and the broader tail around HCC 007 which connects with the off-centered envelope. These structures stand out more clearly in Fig. 13 than in the earlier Fig. 11 because with the MSM we no longer have negative residuals.

Quantitatively, the peak surface brightness of the off-centered envelope is  $\mu_{0,V} = 23.2$  mag arcsec $^{-2}$ , as given by the exponential fit along P.A. = 32°. The average surface brightness in the tail around HCC 026 is  $\mu_V = 24.8 \pm 0.2$  mag arcsec $^{-2}$  in the area enclosed by the blue dashed polygon in Fig. 13. The tail around HCC 007 is brighter on the NE side where  $\mu_V = 24.4 \pm 0.5$  mag arcsec $^{-2}$ , than on the NW side where it is about one magnitude fainter.

We can check with Figure 14 that the NW tail of HCC 007 is not an artifact of residual halo light in NGC 3309. The upper panel of this figure shows that the minor axis profile of this galaxy (P.A. = 320°) is well described by the fitted Sersic profile, whereas additional light is seen along P.A. = 230° and particularly along P.A. = 190° which goes through the brightest part of the NW tail close to HCC 007.

Finally, we show that the morphologies of the substructures seen in the residual image in Fig. 13 are not due to systematic effects in the 2D modeling caused by uncertainties in the background estimates. This concern can be addressed by showing that these substructures are present in two independent datasets, the VLT/FORS1 and 2.2m/WFI images. We have already seen in Sect. 3.2 that the asymmetries in the extracted profiles along P.A. = 32°, 212° are very similar in the two data sets; this confirms independently the presence of the off-centered envelope NE of NGC 3311. The lower panel of Fig. 14 compares the VLT/FORS1 and WFI surface brightness profiles through the fainter NW tail of HCC 007 along P.A. = 190° as seen from the center of NGC 3309. The light excess in the HCC 007 tail is clear in both data sets. Both results are independent of the slight residual gradient described in Sect. 3.2, because this is essentially perpendicular to P.A. = 32° and P.A. = 190°. Finally, we have also carried out 2D GALFIT modeling on the 2.2m/WFI V band image, using the 1D minimal model fit parameters for NGC 3311, and the “allmask” mask shown in Fig. 2 to determine the parameters of NGC 3309. The residual V-band 2.2m/WFI image has a lower S/N than that based on the VLT/FORS1 data. Nonetheless both elongated streams around HCC 026 and HCC 007 are independently confirmed. In the case of HCC 007, only the brighter NE tail is visible in the residual image.

#### 4.4. Luminosities of the substructures in the Hydra I core

We next compute the total luminosity of the off-centered envelope from the flux within the elliptical aperture shown in Fig. 13. We mask stars, dwarf galaxies, and a circular region with  $R = 23''$  centred on NGC 3311. The resulting luminosity in the off-centred envelope is  $L_{V,NE,env} = 1.2 \times 10^{10} (\pm 6.0 \times 10^8) L_\odot^1$ ,

<sup>1</sup> The 1- $\sigma$  error in the luminosity is estimated by integrating the sky rms per pixel over the area enclosed by the elliptical aperture.

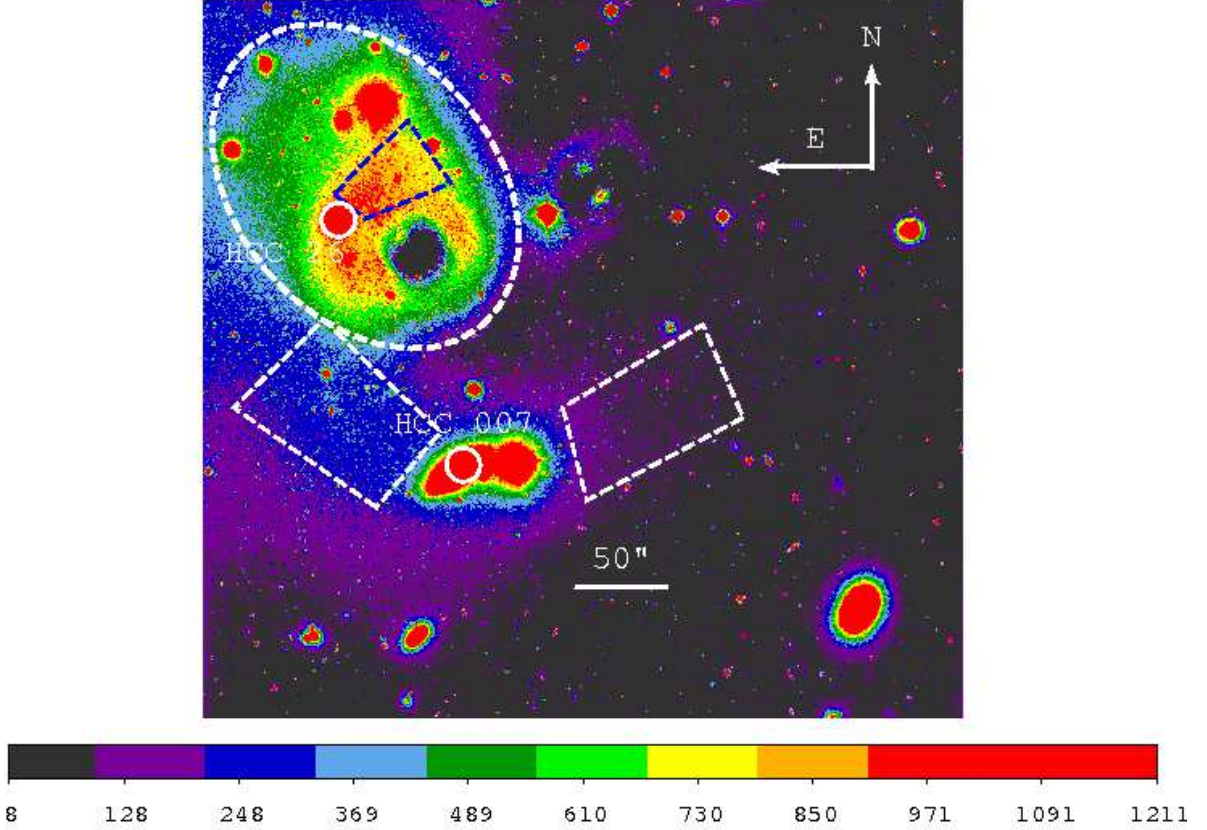


**Fig. 13.** Residual VLT/FORS1 V-band image with respect to the MSM for NGC 3311 and NGC 3309. The white ellipse indicates the extended halo off-centered towards the NE of the bright inner regions of NGC 3311. The most noticeable substructure on top of the extended envelope NE of NGC 3311 is the tidal stream associated with the dwarf galaxy HCC 026. Its NW part is indicated on the image with the blue dashed polygon. At larger radii, and at fainter surface brightness levels, we see a thicker tail around HCC 007; the luminosity in this tail is computed in the areas limited by the white polygons, see Sect. 4.4. The two small objects near the center of the NE polygon may be connected by a possible further small stream; see also Fig. 11. The FoV is  $6'.8 \times 6'.4$ . Colour levels are linear in ADU.

using a distance of 50 Mpc for the Hydra I cluster. This estimate does not include the luminosity of the MSM halo in this region (see also Sect. 5), but it does include the light in the stream around HCC 026, which is seen in addition to the exponential component in Fig. 12.

For comparison, we compute the luminosity of the MSM *i)* within the same elliptical aperture, and *ii)* in the circular annulus between  $R = 23''$  and  $120''$ , by integrating the flux of the GALFIT model output image over the respective areas. The luminosities of the MSM model evaluated in these two regions are  $L_{V,NE,halo} = 2.3 \times 10^{10} (\pm 6.0 \times 10^8) L_{\odot}$  and  $L_{V,halo} = 7.5 \times 10^{10} (\pm 2.0 \times 10^9) L_{\odot}$ . Thus, within the area limited by the elliptical aperture in Fig. 13, the luminosity in the off-centered envelope amounts to 50% of the light in the MSM, while it is only 15% of the total luminosity of the MSM integrated between  $23''$  and  $120''$ .

To estimate the luminosity of the HCC 026 tail we carry out surface photometry in a polygon designed to include most of the NW half of the stream; it is constructed with the *IRAF POLYMARK* and *POLYPHOT* tasks and is shown by the blue dashed polygon in Fig. 13. From the luminosity measured in this polygon we subtract the contribution of the smooth envelope in the same area. The resulting luminosity of the NW part of the stream is  $L_{V,NWstreamHCC\ 026} = 4.8 \times 10^8 (\pm 8 \times 10^7) L_{\odot}$ , which is

equivalent to an apparent magnitude of  $m_{V,streamHCC\ 026} = 16.6$ . Thus the NW stream of HCC 026 contributes about  $\sim 15\%$  of the combined surface brightness of the MSM halo and off-centered envelope at the stream position (see also Fig. 12), consistent with the estimate obtained independently from stellar population analysis in Coccato et al. (2011a). The luminosity in the southern part of the HCC 026 stream is more difficult to disentangle from the diffuse halo, but comparable. The total stream luminosity is clearly several times larger than the total luminosity of the dwarf galaxy HCC 026 itself,  $L_{V,HCC\ 026} = 1.5 \times 10^8 L_{\odot}$  (Misgeld et al. 2008), and if the stream is physically related to HCC 026, a large part of the luminosity of this galaxy has already been tidally dissolved!

In a similar way, we compute the light in the tail emerging from HCC 007. We define two polygons shown by the white dashed boxes in Fig. 13 NE and NW of HCC 007 and carry out the photometry with the *POLYPHOT* task. The apparent V band magnitudes in the two polygons are  $m_v = 14.9$  and  $16.3$  for the NE, NW sides, respectively. At a distance of 50 Mpc, the combined luminosity in the two polygons on the HCC 007 tails is therefore  $L_{V,streamHCC\ 007} = 2.95 \times 10^9 (\pm 510^8) L_{\odot}$ . For comparison, the V band luminosity of HCC 007 from the  $V_0$  magnitude measured in Misgeld et al. (2008),  $V_0 = 14.18 \pm 0.01$ , is  $L_{V,HCC\ 007} = 4.5 \times 10^9 L_{\odot}$ . Thus the ratio between the lumi-

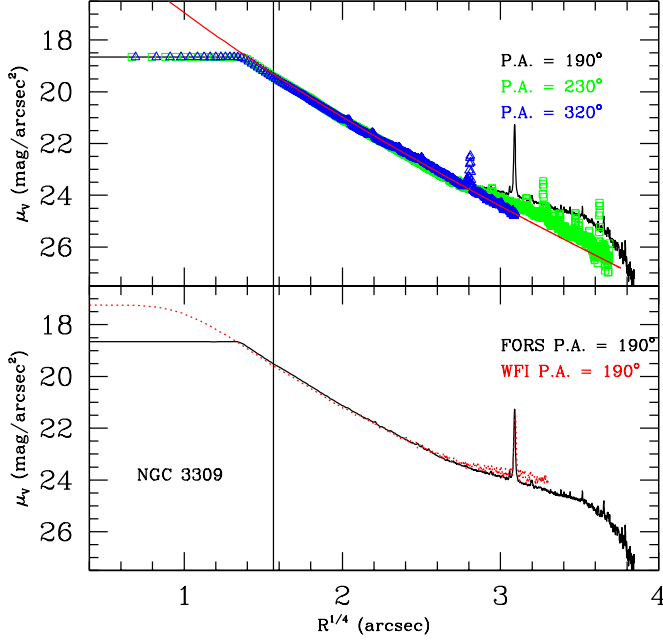


**Fig. 14.** Upper panel: surface brightness profiles extracted in  $5^\circ$  wide cones along the major (P.A. =  $230^\circ$ , green squares), minor axis (P.A. =  $320^\circ$ , blue triangles) and intermediate axis (P.A. =  $190^\circ$ , black line) of NGC 3309, plotted as function of  $R^{1/4}$ . The red continuous line shows the extracted 1D major axis profile for the 2D GALFIT “minimal” symmetric model (MSM) to the light of NGC 3309. While this is a good fit for the minor axis profile at large radii, profiles along P.A. =  $230^\circ$  and P.A. =  $190^\circ$  show additional light, as they go trough the brightest part of the HCC 007 NW stream. Lower panel: surface brightness profile from VLT/FORS1 (black line) and 2.2/WFI (red line) V band images along P.A. =  $190^\circ$ .

osity in the tail polygons and of the S0 galaxy HCC 007 is  $L_{V,\text{streamHCC 007}}/L_{\text{HCC 007}} = 0.66$ . This is obviously a lower limit; especially if the NE tail extends into the off-centered halo of NGC 3311, its luminosity may be substantially larger than estimated with the NE polygon. Thus at least 40% of the original luminosity of HCC 007 have already been dissolved from the galaxy.

In summary, our extensive photometric analysis of the Ks and V band images provides strong quantitative evidence for an extended envelope around NGC 3311 off-centered towards the NE, and for luminous streams around HCC 026 and HCC 007. We now wish to establish the kinematic association of these diffuse structures to their galaxies, with the goal of understanding their origin.

## 5. Long slit spectroscopy for the NGC 3311 outer halo and for the tidal stream of HCC 026

First we investigate whether the presence of the off-centered, extended envelope around NGC 3311 is associated with any clear signatures in the kinematics obtained from deep long slit spectra. In Section 5.1 we discuss the mean LOS velocity and velocity dispersion profiles with respect to the center of NGC 3311. We then describe the link between kinematic and surface brightness features in order to constrain the dynamics of the inner galaxy

and the outer halo. In Section 5.2 we seek spectroscopic evidence for the presence of the tidal tails emerging from HCC 026.

### 5.1. Kinematic signatures of the off-centered envelope around NGC 3311

In Ventimiglia et al. (2010) we already showed that the halo around NGC 3311 for  $R > 15''$  is dynamically hot. The kinematic data for NGC 3311 show an extremely rapid rise from galaxy-typical values of  $\sigma_{\text{LOS}}(R < 15'') \approx 170 \text{ km s}^{-1}$  to velocity dispersions  $\sigma_{\text{LOS}}(50'') > 400 \text{ km s}^{-1}$  dominated by the cluster potential. This study was based on Gemini long slit spectra along P.A. =  $63^\circ$ , and deep VLT/FORS2 long slit spectra centered on the dwarf galaxy HCC 026 with P.A. =  $142^\circ$ . More recently, the VLT/FORS1 spectra along P.A. =  $29^\circ$  published by Richtler et al. (2011) confirmed the large outer velocity dispersion values and the asymmetry of the  $V_{\text{LOS}}$  profiles, but also showed deviations between measurements at different P.A.

The mean LOS velocity  $V_{\text{LOS}}(R)$  profiles along both P.A.s increase outwards from NGC 3311 by  $\sim 100 \text{ km s}^{-1}$  to the NE, while they remain close to the galaxy systemic velocity  $V_{\text{NGC3311}}(R) = 3800 \text{ km s}^{-1}$  to the SW. Thus Ventimiglia et al. (2010) concluded that the NE outer halo has slightly more red-shifted mean LOS velocities,  $V_{\text{halo}} \approx 3900 \text{ km s}^{-1}$ , and is offset by  $\sim +100 \text{ km s}^{-1}$  relative to the NGC 3311 center. The photometric evidence for an offset halo component to the NE of NGC 3311 shown in Fig. 13 suggests that the stars in the offset halo could be responsible for the shift in LOS velocities.

Building on the photometric model derived in Section 4.3, we can check whether either  $\sigma_{\text{LOS}}(R)$  and/or  $V_{\text{LOS}}(R)$  increase at positions where the surface brightness of the extended offset envelope is comparable to or brighter than the surface brightness of the MSM for NGC 3311. In Fig. 15 we illustrate this analysis, comparing kinematic and surface brightness profiles along the galaxy’s approximate major axis (P.A. =  $29^\circ$ , and P.A. =  $32^\circ$ , respectively). Indeed, both  $V_{\text{LOS}}$  and  $\sigma_{\text{LOS}}$  increase as the surface brightness of the offset envelope increases from  $R \approx 15''$  outwards. In particular, the  $V_{\text{LOS}}$  values are more red-shifted on the NE side of the galaxy center than either at the center or in the SW region. However, this asymmetry peaks at  $R \approx 30''$  and does not closely follow the estimated relative surface brightness contribution of the off-centred envelope.

The outermost measurement from (Ventimiglia et al. 2010) of  $V_{\text{LOS}} = 3835 \text{ km s}^{-1}$  and  $\sigma_{\text{LOS}} = 429 \text{ km s}^{-1}$  at  $R = 100''$  is relevant for this discussion. These values are measured for a 1D spectrum extracted from a region in the NGC 3311 halo that is only weakly affected by the off-centred envelope; the orange-dashed line in Figure 16 shows the location of this slit region on the image. These measurements therefore suggest that the symmetric halo is *hot* and *approximately at the galaxy systemic velocity*, and that the off-centred envelope is responsible for shifting the velocities measured in the NE quadrant of the NGC 3311 halo to more red-shifted values. We will return to this issue in Section 6.

### 5.2. Kinematics signatures of the tidal stream around HCC 026

We wish now to confirm that the stream-like substructure in the diffuse envelope NE of NGC 3311 is physically associated with the dwarf galaxy HCC 026. The goal is to see whether we can detect absorption line features in the spectra at the position of



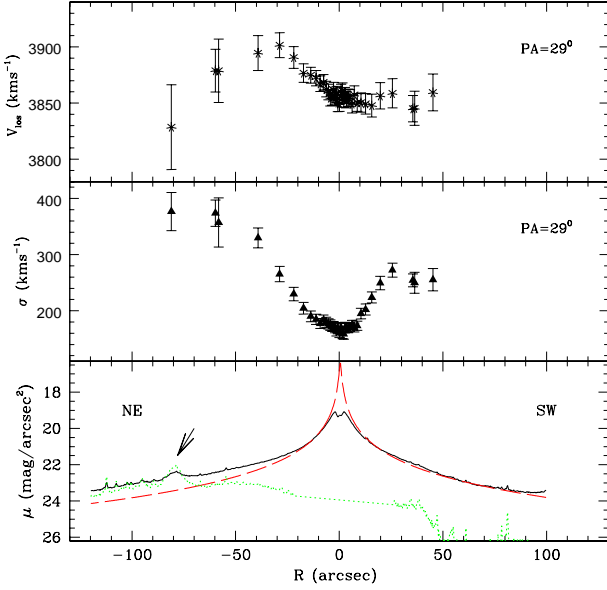


**Fig. 15.** Asymmetric kinematics and light distribution of the off-centered envelope around NGC 3311. Lower panel: the full black line shows the extracted surface brightness profile from the VLT/FORS1 V band image along P.A. = 32°, the red dashed line shows the Sersic profile ( $n = 10.5, R_e = 850''$ ) of the MSM described in Sect. 4.3, and the green dashed line shows the contribution from the off-centered outer envelope along this P.A. The arrow indicates the dwarf galaxy HCC 027. Middle and upper panels: LOS velocity dispersion ( $\sigma_{\text{LOS}}$ , triangles) and velocity measurements ( $V_{\text{LOS}}$ , asterisks) along P.A. = 29° from Richtler et al. (2011) (P.A. = 29° shown as  $R < 0$ ).

the tidal stream, in addition to the absorption lines from the stars in this part of the dynamically hot halo of NGC 3311.

We use the deep long slit spectroscopic observations of the NGC 3311 halo carried out by Ventimiglia et al. (2010) with FORS2 on VLT-UT1. These spectra extend over the wavelength range 4655 Å – 5955 Å and include absorption lines from H $\beta$ , Mg I ( $\lambda\lambda 5167, 5173, 5184$  Å) and Fe I ( $\lambda\lambda 5270, 5328$  Å). They were acquired with a 6'.8 arcmin long-slit of width 1''.6, and GRISM 1400+V, giving an instrumental dispersion of 0.64 Å pixel<sup>-1</sup> and a spectral resolution of  $\sigma = 90$  km s<sup>-1</sup>. The long slit was centered on the dwarf galaxy HCC 026 at  $\alpha = 10^{\text{h}}36^{\text{m}}45.85^{\text{s}}$  and  $\delta = -27^{\circ}31'24.2''$  (J2000), with a position angle P.A. = 142° so that it passes through the photometric stream. HCC 026 itself is seen in projection onto the NGC 3311 halo. The slit geometry is shown in Figure 16. Eight exposures of 1800 sec each were taken (in total 4 hrs). In addition to the deep spectra, the standard G8III star HD102070 and the spectrophotometric standard star EG 274 were also observed with the same set-up. The data reduction followed standard procedures as described in Ventimiglia et al. (2010). The final deep 2D spectrum was then used to construct radial profiles of the velocity dispersion and mean LOS velocity for the halo of NGC 3311 from measurements at various positions along the slit.

Here we want to additionally detect in the spectrum the absorption lines of the stream superposed onto the main absorption features of the hot NGC 3311 halo. We expect these secondary absorption lines to have strengths of about 15% of those for the NGC 3311 halo, on the basis of the photometry carried

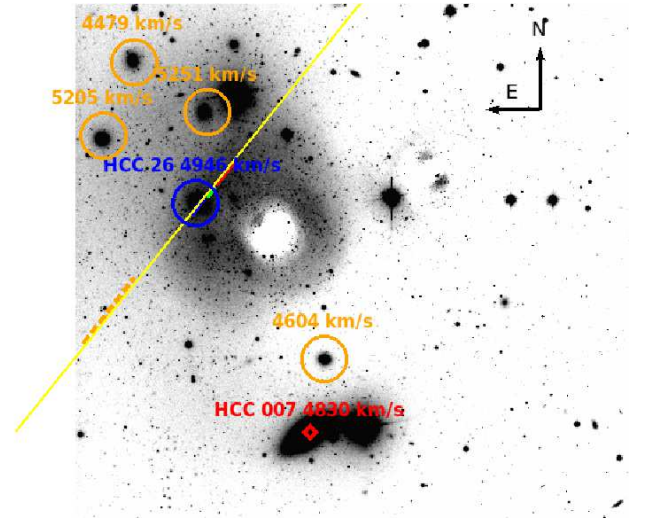


**Fig. 16.** Location of dwarf galaxies and long slit on the residual VLT/FORS1 V-band image from Fig. 13. Here the orange circles indicate the dwarf galaxies within 100 kpc of the NGC 3311 center; their velocities are reported on the image. The cyan circle shows the dwarf galaxy HCC 026, and the red diamond indicates HCC 007. The object to the right of HCC 007 is a foreground star. The yellow line centered on HCC 026 at P.A. = 142° illustrates the position and orientation of the long slit used for the kinematic measurements in Ventimiglia et al. (2010) and in this paper. The orange-dashed section of the slit identifies the area where the  $V_{\text{LOS}}, \sigma$  measurements at  $R = 100''$  were taken (Ventimiglia et al. 2010); see Sect. 5.1. The red and green parts of the line depict the slit sections used to measure the mean velocity of the tidal stream. The FoV is  $5'.1 \times 2'.8$ ; North is up and East to the left.

out in Sect. 4.3; see Figs. 12, 13, and 15. If the sub-component projected on the outer halo is a tidal stream emerging from HCC 026, we expect its absorption lines to occur at significantly different recession velocity from those of the NGC 3311 diffuse halo ( $V_{\text{halo}} = 3921$  km s<sup>-1</sup>). This is based on the fact that all of the dwarf galaxies seen at this location, including HCC 026, have recession velocities of order 5000 km s<sup>-1</sup>, see Table 3 and Ventimiglia et al. (2011).

We first extract the light profile along the slit and identify those regions where the continuum is bright enough to provide suitable S/N for the kinematic measurements. We can identify only two such regions to the North-West of HCC 026: region I - 7'' wide (30 pixels)- and region II - 18'' wide (75 pixels). These are indicated by the green and red slit sections in Figures 16 and 17. All the flux in each of these regions is co-added to reach  $S/N \approx 20$  in the continuum for the final one-dimensional (1D) extracted spectra. We must be aware that co-adding all the signal from an extended portion of the slit causes a broadening of the absorption lines, but this does not affect our goal, which is the detection of a secondary absorption line component at a different LOS velocity from that associated with the hot halo component.

To measure the stellar kinematics, we restrict ourselves to the central wavelength range  $4800 \text{ Å} < \lambda < 5800 \text{ Å}$  of the extracted 1D spectrum, and use the “penalized pixel-fitting” method (PPXF Cappellari & Emsellem 2004). In the PPXF method, stellar template stars from the MILES library (Sanchez-Blazquez et al. 2007) are combined to fit the 1D spectrum while simultaneously determining the mean LOS velocity and velocity dispersion from the absorption lines. From the best

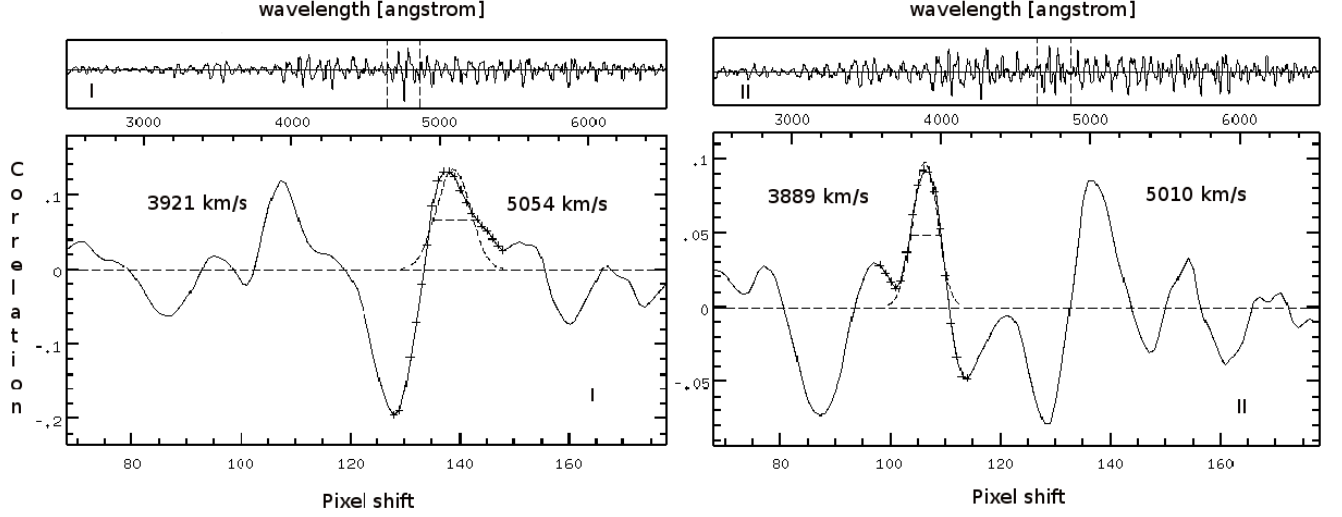


**Fig. 19.** Cross correlation functions used for kinematic measurements in two slit sections. *Upper panels:* Fourier cross-correlation functions computed between the residual (excess) spectra and the spectrum of the G dwarf star HD102070 for spectrum I (left) and II (right). *Lower panels:* Enlarged view of the Fourier cross-correlation function peaks. The double peaks in both Fourier cross-correlation functions indicate the presence of two sets of absorption line features at different velocities in the residual spectra. The more red-shifted peaks in the Fourier cross-correlation are at velocities  $V_{\text{LOS},1} = 5054, 5010 (\pm 55) \text{ km s}^{-1}$ , and the secondary bluer peaks are at  $V_{\text{LOS},2} = 3921, 3889 (\pm 55) \text{ km s}^{-1}$ .

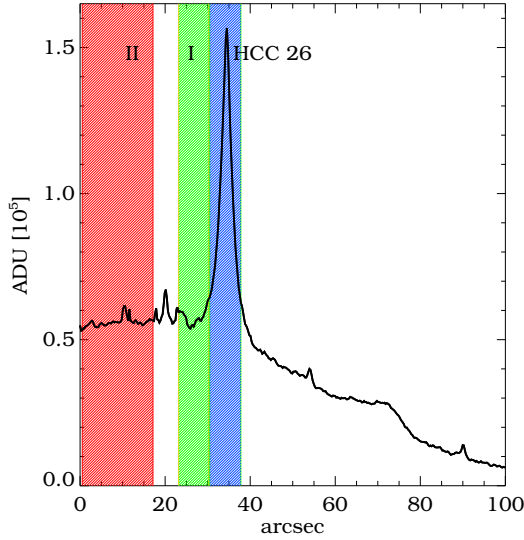


**Fig. 17.** Light profile along the slit centered on HCC 026, with the different color-shaded areas indicating the slit sections used for the extraction of the 1D spectra of HCC 026 (blue) and the tidal stream (green and red). Left is SE of HCC 026, right is NW.

PPFX fit to the co-added spectrum we obtain values for these kinematic parameters which are consistent with the halo kinematics measured by Ventimiglia et al. (2010), as well as a best-fit stellar template for the halo of NGC 3311.

From the photometry carried out in Section 4.3, the luminosity from the tidal stream amounts to  $\sim 15\%$  of the total light in the region sampled by this spectrum. Attempting a direct spectral decomposition of the stellar halo of NGC 3311 and the light excess as in Coccato et al. (2011b) was unsuccessful. To be able to detect the weak kinematic signal from the excess of light, we

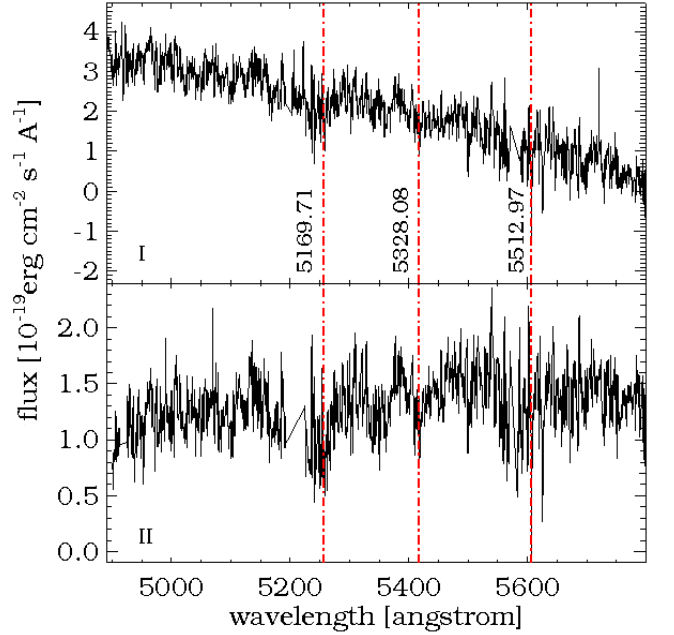


**Fig. 18.** 1D wavelength and flux calibrated residual spectra I (upper panel) and II (lower panel), extracted at the position of the light excess. These 1D spectra are obtained by subtracting a template model of the NGC 3311 halo from the extracted 1D spectra. The vertical dash-dotted lines indicate the locations of the main absorption features whose rest frame wavelengths are also reported on the figure.

therefore need to subtract the main halo contribution. We achieve this by taking the best-fit stellar template spectrum obtained by PPFX for the total extracted science spectrum, multiply it by a suitable fraction (0.85) and subtract it off the extracted spectrum.

This procedure when applied to the 1D spectra I and II leaves the residual spectra shown in Figure 18.

Clearly, the S/N of the residual spectra is not high enough for a direct pixel fitting, although the main absorption features are readily identified, and we must now use a different approach. We use the *RV.FXCOR* task in IRAF to identify the velocity components in the residual spectrum; this task implements the Fourier cross-correlation technique of Tonry & Davis (1979). The upper panels of Figure 19 show the Fourier cross correlation functions computed with *RV.FXCOR* between the residual 1D spectra I and II and the extracted 1D spectrum of the star HD102070. All spectra have their continuum fitted and subtracted-off, and only the wavelength interval  $4800\text{\AA} < \lambda < 5800\text{\AA}$  is used.

In the lower panels of Fig. 19, the region centered around the two strongest correlation peaks is enlarged. This reveals the presence of two components at different velocities in both spectra: the strongest peak is found at  $5054\text{ km s}^{-1}$ ,  $5010\text{ km s}^{-1}$  and a second peak is detected at  $3931\text{ km s}^{-1}$ ,  $3889\text{ km s}^{-1}$ , for spectrum I and II respectively. The error in each velocity measurement is  $\pm 55\text{ km s}^{-1}$ . The height of both peaks in the cross correlation spectrum is  $\sim 2 - 3$  times the amplitude of the noise; we therefore judge these signals to be significant. The bluer velocity peaks correspond to a component from the extended halo light that is still present in the residual spectra at an average LOS velocity of  $3905\text{ km s}^{-1}$ , see also Sect. 5.1. The peaks at more redshifted LOS velocities indeed provide evidence for a second component at  $\Delta V \simeq +1200\text{ km s}^{-1}$  relative velocity with respect to the systemic velocity of NGC 3311 ( $V_{\text{NGC3311}} = 3800\text{ km s}^{-1}$ ), and  $\Delta V \simeq +1100\text{ km s}^{-1}$  relative to the halo ( $V_{\text{halo}} = 3921\text{ km s}^{-1}$ ). The average LOS velocity obtained by combining the measurements from spectra I and II is  $5032 \pm 38\text{ km s}^{-1}$ . For comparison, the LOS velocity of HCC 026 is  $4946 \pm 4\text{ km s}^{-1}$  (Ventimiglia et al. 2010).

In summary, the stars in the stream NE of HCC 026 have a LOS velocity very similar to that of HCC 026 itself but  $\Delta V \simeq +1200\text{ km s}^{-1}$  different from the systemic velocity of NGC 3311. This is a necessary condition for the stream around HCC 026 being a tidal stream, but may still be consistent also with the stream stars being part of a shell which was stripped from a larger galaxy together with HCC 026. However, combining our kinematic result with the result of Coccato et al. (2011a) that the stellar population at the NW stream position is more metal poor than in the surrounding outer halo, consistent with the superposed stream stars having similar metallicity as the dwarf galaxy HCC 026 itself, makes a strong case that the stars in the stream were indeed tidally stripped from HCC 026.

## 6. Correspondence between surface brightness components and kinematical structures measured with planetary nebulae, and the velocities along the HCC 007 tail

To begin with, we summarize the results from observations of PN kinematics in the Hydra I cluster core, in order to see how they may help in understanding the physical structures identified in the photometry. In Ventimiglia et al. (2011), we measured LOS velocities for 56 PNs in a  $6.8' \times 6.8'$  field covering the central  $(100\text{kpc})^2$  of the Hydra I cluster, using multi-slit imaging spectroscopy (MSIS Gerhard et al. 2005; Arnaboldi et al. 2007). We identified different velocity components in the PN LOSVD and described their spatial distributions. In brief, we found:

- A broad, asymmetric central velocity component in the PNs LOSVD, peaked at  $\sim 3100\text{ km s}^{-1}$  and with  $\sigma \simeq 500\text{ km s}^{-1}$ .

The spatial distribution of these PNs has significant substructure, depending on the LOS velocity. It is not clear whether this component traces the symmetric halo around NGC 3311.

- A minor blue-shifted velocity component, centered at  $\sim 1800\text{ km s}^{-1}$ , whose PNs have an elongated distribution along the North/South direction. There is no galaxy with similar velocity inside the  $6.8' \times 6.8'$  field centered on NGC 3311, but two such galaxies are located near the perimeter of the field. The association of these with the blue-shifted PNs is possible but unclear, however.
- A narrow red-shifted velocity component, around  $V_{\text{LOS}} \simeq 5000\text{ km s}^{-1}$ . These red-shifted PNs show a concentration in the NE quadrant of NGC 3311, and are correlated spatially and in LOS velocity with a group of dwarf galaxies, which are observed within  $(100\text{ kpc})^2$  of NGC 3311.

In Figure 20, we plot the PNs associated with the red-shifted peak of the PN LOSVD (Ventimiglia et al. 2011) on the residual VLT/FORS1 V band image with respect to the MSM for NGC 3311. This shows that a major fraction of these red-shifted PNs are concentrated in the NE quadrant where the offset halo is found. We count 10 PNs superposed on the offset envelope. Their average LOS velocity is  $V_{\text{redPNs,LOS}} = 5095\text{ km s}^{-1}$  and  $\sigma_{\text{redPNs,LOS}} = 521\text{ km s}^{-1}$ . The average LOS velocity is similar to that of HCC 026 ( $V_{\text{HCC026}} = 4946\text{ km s}^{-1}$ ) and to the value for the second component measured in Sect. 5.2 ( $5032\text{ km s}^{-1}$  average). With a relative offset of  $1200\text{ km s}^{-1}$  from NGC 3311 and a contribution of  $\simeq 15\%$  to the surface brightness, the shift in the predicted mean velocity would be of order  $180\text{ km s}^{-1}$ , consistent with the measured value. However, we found in Sect. 4.4 that the off-centered envelope contributes  $\sim 30\%$  of the surface brightness in the NE region, and this value is consistent with the value indicated at the HCC 026 position in Figs. 12, 15. Thus, while from their spatial location the red-shifted PNs appear to trace the off-centered envelope, it is not clear whether they trace all the stars in it.

Therefore, from the off-centered envelope's luminosity estimated in Sect. 4.4,  $L_{\text{V,NE,env}} = 1.2 \times 10^{10} (\pm 6.0 \times 10^8) L_{\odot}$ , we can derive an upper limit for the luminosity specific PN number  $\alpha$  for this stellar population. The measured value is  $\alpha = 1/1.2 \times 10^9\text{ PN } L_{\odot}^{-1}$ ; once we correct this number for the limiting magnitude of these MSIS observations  $\alpha_{\text{TOT}} = 82 \times \alpha$  (see Ventimiglia et al. (2011) for further details), we obtain  $\log(\alpha_{\text{TOT}}) = -7.18$ . This value for  $\alpha_{\text{TOT}}$  is similar to that for old stellar populations which are observed in the M31 bulge and S0s galaxies (Buzzoni et al. 2006).

For the symmetric halo of NGC 3311 the  $\alpha$  parameter must be lower. Within  $23'' < R < 120''$ , we count 12 PNs from the central velocity component (Ventimiglia et al. 2011). If these trace the total luminosity of the symmetric halo,  $L_{\text{V,halo}} = 7.5 \times 10^{10} (\pm 2.0 \times 10^9) L_{\odot}$ , the measured  $\alpha = 1/6.2 \times 10^9\text{ PN } L_{\odot}^{-1}$  and the corresponding  $\log(\alpha_{\text{TOT}})$  is  $-7.87$ , a factor 5 lower than the value for the stellar population in the offset envelope. In fact, the LOSVD of the central PN component is quite axisymmetric, and very few PNs at the systemic velocity of NGC 3311 are found on the inner symmetric halo. Thus the  $\log(\alpha_{\text{TOT}})$  for this component may be even lower.

Superposed the off-centered envelope, there are two tidal streams in the Hydra I core; they are shown in Figs. 11 and 13. In Sect. 5.2 the direct measurement of  $V_{\text{LOS}}$  of the stream around HCC 026 is  $5032 \pm 38\text{ km s}^{-1}$ , and the systemic velocities of HCC 026 and HCC 007 are  $v_{\text{sys}} = 4946\text{ km s}^{-1}$ ,  $v_{\text{sys}} = 4830\text{ km s}^{-1}$  respectively. Three of the PNs plotted in Figure 20 are consistent with being located on the backward HCC 007 stream



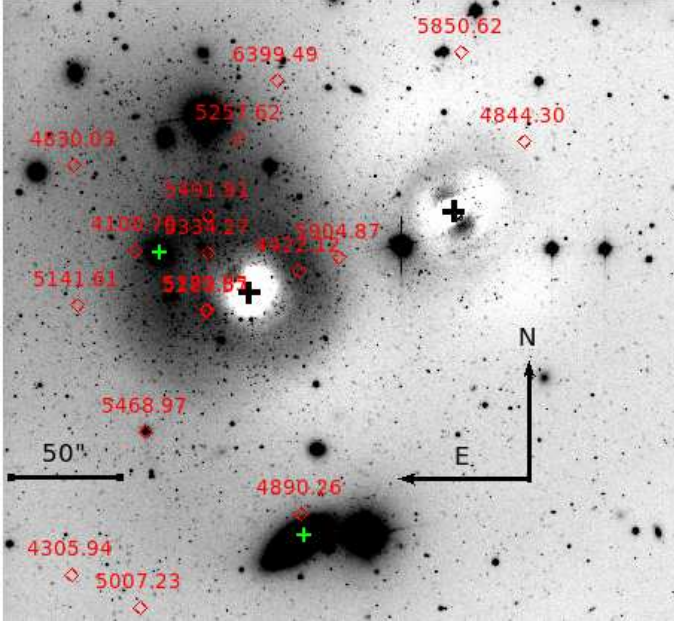


**Fig. 20.** Positions and velocities of PNs (red diamonds, labels indicate the PNs'  $V_{\text{LOS}}$  in  $\text{km s}^{-1}$ ) associated with the red peak at  $5000 \text{ km s}^{-1}$  in the PN LOSVD of the Hydra I cluster, from Ventimiglia et al. (2011). The red peak PNs are superposed on the residual V-band image, which shows the substructures in the diffuse light in the Hydra I cluster core. The black crosses indicate the position of NGC 3311 (center) and NGC 3309 (upper right), respectively. The green crosses indicate HCC 026 and HCC 007. The FoV is  $5'.2 \times 4'.9$ .

(one is on the polygon used to estimate the luminosity). These indicate a systematic velocity gradient along the stream, increasing from  $4830 \text{ km s}^{-1}$  east of the off-centered envelope to a maximum of  $5470 \text{ km s}^{-1}$  near the closest approach to NGC 3311, and decreasing again to  $4890 \text{ km s}^{-1}$  near HCC 007 itself.

Assuming that the stellar population in these streams is similar to that in the off-set envelope, we would expect  $2 \pm 1$  PN in the polygon on the NE tail of HCC 007, and no PNs on the SE tail or on the stream around HCC 026. In Figure 20, we count one PN associated with the corresponding part of the HCC 007 stream, which is consistent with the prediction. There is not enough light in the stream around HCC 026 to expect any PN to be detected within the limiting magnitude of the Ventimiglia et al. (2011) survey.

## 7. Discussion

### 7.1. The peculiar outer halo of NGC 3311

*Outer halo or intracluster light?* – Based on V-band photometry out to  $\sim 100''$  ( $\sim 25 \text{ kpc}$ ), the outer halo of NGC 3311 can be represented by a symmetric Sersic model with large  $n \approx 10$ , and an additional off-centered component with centroid shifted by about  $50''$  to the NE (Sect. 4). The off-centered component can be described by a (flatter) exponential profile. However, it is not the extended light profile which distinguishes this central cluster galaxy from other luminous elliptical galaxies, but its very steeply rising velocity dispersion profile (VDP)  $\sigma(R)$ . From a central value of  $\sim 170 \text{ km s}^{-1}$ , the VDP rises to  $\sigma \approx 230 \text{ km s}^{-1}$  at  $R = 15'' \approx 3.7 \text{ kpc}$ , and then on to  $\sigma = 300 - 450 \text{ km s}^{-1}$  at  $R = 50'' \approx 12 \text{ kpc}$  (Ventimiglia et al. 2010; Richtler et al. 2011). The steep rise of the velocity dispersion profile corresponds to a

steep increase in the enclosed mass. Within  $R = 20 \text{ kpc}$ , the total dark matter mass inferred from X-ray observations is  $\sim 10^{12} M_{\odot}$  (Hayakawa et al. 2004). Thus NGC 3311 is located at the center of the dark matter cusp of the Hydra I cluster.

In the NW region dominated by the off-centered halo component, the velocity dispersion is particularly high ( $\sim 450 \text{ km s}^{-1}$ ), about 60% of the galaxy velocity dispersion in the cluster core (Ventimiglia et al. 2010). Its mean LOS velocity is also shifted by  $\sim 100 \text{ km s}^{-1}$  with respect to NGC 3311. Many PNs located on the off-centered envelope move at LOS velocities of  $+1200 \text{ km s}^{-1}$  with respect to the NGC 3311 center (Ventimiglia et al. 2011), but also the LOSVD of the 'central PN component' of Ventimiglia et al. (2011) is quite asymmetric. The off-centered envelope may therefore equally well be considered as part of the ICL in the cluster core; because of the steeply rising VDP, distinguishing outer halo from ICL is difficult (see Dolag et al. 2010).

*Dynamically hot outer halos in other BCGs?* – A galaxy with a dynamically hot outer halo similar to NGC 3311 is NGC 6166, the cD galaxy in the cluster A2199 (Kelson et al. 2002). In this system, the velocity dispersion first decreases from the central value of  $300 \text{ km s}^{-1}$  to  $200 \text{ km s}^{-1}$  within a few kiloparsecs, and then steadily rises to  $660 \text{ km s}^{-1}$  at a radius of  $60 \text{ kpc}$ , nearly reaching the velocity dispersion of the cluster ( $\sigma_{\text{A2199}} = 775 \pm 50 \text{ km s}^{-1}$ ). This is similar but less extreme than the case of NGC 3311 studied here, which does not show the central decrease. However, such dynamically hot outer halos in BCGs are rare: e.g., for NGC 1399 in the Fornax cluster (McNeil et al. 2010), NGC 4874 and NGC 4989 in Coma (Coccato et al. 2010a) the outer VDPs are flat, while for M87 in the Virgo cluster the VDP first rises out to  $250''$  and then falls steeply (Doherty et al. 2009; Murphy et al. 2011).

*Asymmetry in X-ray observations of the Hydra I cluster core.* – Independent evidence for asymmetries in the Hydra I cluster center comes from Chandra and XMM observations (Hayakawa et al. 2004, 2006). These authors report about an extended emission  $\sim 1'.5$  in the direction NE from NGC 3311 relative to the iso-surface brightness contours further out, with an angular scale of about  $1.5'$ , see Fig. 2 in Hayakawa et al. (2004) and Fig. 5 in Hayakawa et al. (2006). The X-ray surface brightness maps show a morphology reminiscent of the off-centered halo in the stellar light distribution. The extended X-ray emission NE of NGC 3311 is also the brightest among several high metallicity regions in the Hydra I cluster, and its associated gas mass is larger than that in the compact X-ray halo of NGC 3311. Hayakawa et al. (2004) interpret this high metallicity region  $1'.5$  to the NE of NGC 3311 as the result of gas stripping of NGC 3311, which would imply a relative motion of NGC 3311 with respect to the surrounding outer halo. It may be possible that the collision with the dark matter halo of the group including HCC 007 could have induced such a relative motion; this requires further study.

*Off-centered outer envelopes in BCGs.* – Separate outer components in BCGs are frequent; the work of Gonzalez et al. (2005) for a sample of 24 clusters shows that a two component fit to the light profiles of BCGs provides an improved match to the data, and that the two photometric components are misaligned in 60% of the sample. Gonzalez et al. (2005) reported also the case of Abell 1651, where the two components have different centers, with the outer component off-centered by about  $15 \text{ kpc}$  in linear distance. This is similar to the separation between the center of the off-centered envelope described in Sect. 4, and also the center of the extended X-ray emission, from the inner parts of NGC 3311.

*Stellar population in the outer halo of NGC 3311.* – Coccato et al. (2011a) measured the line strength indices for the stellar population in the NGC 3311 halo along a  $6'.8$  slit centred on HCC 026 and with P.A.= $142^\circ$ . These measurements show the effect of the stars in the HCC 026 tail: in this region, the metallicity is lower,  $[\text{Fe}/\text{H}] = -0.73 \pm 0.06$ , compared to the average value for the outer halo away from the tail, where  $[\text{Fe}/\text{H}]_{\text{halo}} = -0.34 \pm 0.05$ . The metallicity in the tail region is consistent with a  $\sim 20\%$  contribution of stars with the metallicity of HCC 026. Unfortunately, in the halo region away from the HCC 026 tail, these data do not have sufficient S/N to test whether the stars in the offset envelope are a different stellar population from those in the symmetric halo.

## 7.2. Tidal tails and streams around NGC 3311

*Comparison of tails in Hydra I with those around other galaxies.* – It is relevant to compare the luminosities of the streams in the Hydra I core with those observed in the halos of bright ellipticals in the Virgo cluster by Janowiecki et al. (2010). The HCC 026 stream identified here with total luminosity slightly below  $10^9 L_{\odot,V}$  is significantly brighter than any of the Virgo streams, and the HCC 007 stream is several times more luminous still. Also, the tidal streams seen around the Virgo cluster ellipticals have much fainter peak surface brightness (brightest:  $\mu_v = 25.7 \text{ mag arcsec}^{-2}$ ; average:  $\mu_v = 27.6 \text{ mag arcsec}^{-2}$ ) than those measured in the Hydra I streams, which are  $\mu_v = 24.8 \text{ mag arcsec}^{-2}$  for the HCC 026 stream and  $\mu_v = 24.4 \text{ mag arcsec}^{-2}$  for the HCC 007 stream.

Streams with as low surface brightness as those observed in Virgo would not be detectable in our Hydra images, thus could easily be abundant in this region. In fact, the two small objects approximately near the middle of the polygon on the NE stream of HCC 007 in Fig. 13 could be connected by a small stream within the HCC 007 tail, as suggested especially by the right panel of Fig. 11. This small stream, if confirmed, would have a luminosity more similar to the Virgo streams, albeit a higher surface brightness.

We can expand this comparison to the streams around bright local elliptical galaxies analyzed by Tal et al. (2009). The Hydra I streams are detected at radii larger than  $\sim 23 \text{ kpc}$  from the center of NGC 3311, and the HCC 007 tail reaches at least  $110 \text{ kpc}$  in total projected length, see the measurement in Sect. 4.2. These numbers for the Hydra I streams are consistent with the average radius of occurrence of the streams studied by Tal et al. (2009), and the linear extent of some of them. Unfortunately, Tal et al. (2009) do not give luminosities for their streams.

*The streams are tidal tails.* – The streams emerging from HCC 026 and HCC 007 can be interpreted as the result of tidal disruption. In the case of HCC 007, the sheer size of the stream (the two tails together span  $\sim 85 \text{ kpc}$ ) is difficult to explain by any other model. For HCC 026, the similar LOS velocity of the stream with the galaxy HCC 026 could still allow a model in which the stream stars are part of a shell which was stripped from a larger galaxy together with HCC 026. However, Coccato et al. (2011a) showed that the metallicity obtained with a single stellar population model in the stream region is lower than in the diffuse stellar halo of NGC 3311 away from the stream, and that this lower metallicity value is consistent with a composite population of stars from HCC 026 and stars from the stellar halo of NGC 3311 in approximately the proportion implied by the surface brightnesses of both components. This makes a strong case that the stars in the HCC 026 stream were indeed tidally stripped

from HCC 026. It also shows that a fruitful way to investigate the origin of the diffuse light features in Hydra I and elsewhere is to measure stellar population parameters from deep spectroscopy.

Given their redshifted velocities, both the HCC 007 and HCC 026 streams would likely be located now on the distant side of the Hydra I cluster core, with their stars being on slightly different orbits than the galaxies they were once bound to.

*Comparison with simulated tails.* – The overall morphology of the two streams in the Hydra I cluster core is similar to those of tidal streams in the simulation investigated by Rudick et al. (2009) to study the formation of intracluster light. In particular, the tidal streams in their case G1 reproduce one characteristic property of the streams discovered here, especially for HCC 007, that one side of the stream is significantly brighter than the other. In the simulation of Rudick et al. (2009), the  $\sim 200 \text{ kpc}$  long tidal arms in G1 formed as a consequence of the interaction of a disk galaxy with the cluster cD, with a pericenter distance of  $\sim 100 \text{ kpc}$ . Most of the stars in the tidal streams in this system were unbound from the disk galaxy shortly after the pericentre passage, and once formed, the streams decay in  $\sim 1.5$  orbital times. The fact that tidal streams are visible around HCC 026 and HCC 007 thus indicates that both galaxies have recently passed the pericenters of their orbits.

## 7.3. A group of galaxies in disruption in the Hydra I cluster core

*All the galaxies in disruption.* – As already reported by Ventimiglia et al. (2011), there are no galaxies in the Hydra I core at cluster-centric radii ( $< 100 \text{ kpc}$ ) with velocities around the cluster systemic velocity. However, several dwarf galaxies at high velocities  $V_{\text{LOS}} \geq 4500 \text{ km s}^{-1}$  and the S0 galaxy HCC 007 are located in this region. In Table 3 we list the sky coordinates, apparent total V-band magnitudes, and LOS velocities for these galaxies from Misgeld et al. (2008). These galaxies are part of a well-defined cluster substructure both in velocity and spatial distribution, as already commented by Ventimiglia et al. (2011) and shown in Figure 16. For two of these galaxies, HCC 026 and HCC 007 we have been able to detect tidal tails, showing that they are being disrupted by the tidal field near the cluster center. For the others, the tidal effects may not yet be strong enough to have lead to detectable tidal tails, or their tails have dispersed below the detection limit. Independent of this, the observed tidal streams are the consequence of the recent infall of a cluster substructure containing the galaxies at  $V_{\text{LOS}} > 4500 \text{ km s}^{-1}$ .

*Where have the central galaxies gone?* – We now return to the observed absence of galaxies at cluster-systemic velocity in the central  $100 \text{ kpc}$  around NGC 3311 (a similar result was found in the NGC 5044 group, Mendel et al. (2009)). A plausible explanation is that such galaxies are no longer seen in the central region of the cluster because they were all disrupted in the past during close encounters with the central galaxy NGC 3311 and with the dark matter cusp at the cluster center (Faltenbacher & Mathews 2005). In this case, their former stars would now be part of the diffuse stellar component in the Hydra I core, including the halo around NGC 3311. It is interesting to ask whether most of the stars in the outer halo could have originated from disruption of small galaxies in the way that seems to be currently on-going, or whether the majority of the halo stars come through a different channel, the tidal disruption of the halos of massive elliptical galaxies prior to merging with the cluster cD (Murante et al. 2007; Puchwein et al. 2010). Again, analysis of the stellar population properties of dwarf galaxies and

Galaxy	$\alpha(2000)$ [h:m:s]	$\delta(2000)$ [°:':"]	$M_V$ [mag]	$v$ [km s <sup>-1</sup> ]
HCC 019	10:36:52.573	-27:32:16.34	16.91	5735±55
HCC 022	10:36:40.373	-27:32:57.68	18.23	4605±37
HCC 023	10:36:48.911	-27:30:01.49	18.07	4479±44
HCC 024	10:36:50.140	-27:30:46.20	17.75	5270±32
HCC 026	10:36:46.000	-27:31:25.10	17.87	4946±04*
HCC 027	10:36:45.700	-27:30:31.30	18.48	5251±89
HCC 007	10:36:41.200	-27:33:39.60	14.18	4830±13

**Table 3.** Dwarf galaxies in the NGC 3311 field. Magnitudes and line-of-sight velocities are from Misgeld et al. (2008). (\*) value from Ventimiglia (2011), Ph.D. Thesis.

of the outer halo stars is important for answering this question (Coccato et al. 2010b, 2011a).

*Phase-mixing and formation of ICL from the tidally dissolved stars.* – Assuming that the interaction with NGC 3311 and the Hydra I cluster core ultimately disrupts the dwarf galaxies seen close to NGC 3311 completely, all of their stars would phase-mix and distribute in the central cluster potential. Converting the uni-directional velocity of their orbits of now  $\sim 1200$  km s<sup>-1</sup> relative to NGC 3311 to  $3\sigma_{\text{eq}}^2$ , the resulting  $\sigma_{\text{eq}} \simeq 700$  km s<sup>-1</sup>. This would be somewhat increased by adding the contribution from the unknown transverse velocities. On the other hand, some of the kinetic energy of these stars would be converted to potential energy during the phase-mixing, lowering the final  $\sigma_{\text{eq}}$ . For comparison, the velocity dispersion of the NGC 3311 halo near the current position of HCC 026 is  $\sigma_{\text{halo}} \simeq 400$  km s<sup>-1</sup>. This suggests that the stars from the galaxies that are presently tidally disrupted will end up at larger radii than their current position, and with somewhat larger dispersion than the observed  $\sigma_{\text{halo}} \simeq 400$  km s<sup>-1</sup>. I.e., they will end up in the outermost halo and intracluster light around NGC 3311 and in the Hydra I cluster core.

## 8. Summary and conclusions

In this work we extend our investigation of the properties and origin of the diffuse light in the Hydra I cluster. Combining surface photometry with kinematic information from long slit and planetary nebula (PN) data, we find an off-centered, diffuse outer halo around the central galaxy NGC 3311, and show that at least two galaxies are currently disrupted in the cluster core, adding their stars to the outer halo and intracluster light around NGC 3311. More specifically, our results are as follows:

Structural parameters are derived for the two giant elliptical galaxies in the cluster core, NGC 3309 and NGC 3311, using V-band imaging data obtained at the ESO/MPI 2.2m telescope and archival VLT/FORS1 V band and 2MASS Ks data. While the light distribution of NGC 3309 is reproduced by a single Sersic profile, that of NGC 3311 is characterized by several components. Outside the nuclear regions which are affected by a dust lane and by bright luminous knots, the bright regions within 30'' follow an  $R^{1/4}$  law in the Ks band. In the deeper V band data, these regions together with the symmetric part of the outer halo can be described by a Sersic law with  $n \simeq 10$ .

The residual image, obtained after subtracting the two-dimensional model of the two bright galaxies, shows an additional extended envelope centered at  $\sim 80''$  to the North-East of NGC 3311. This off-centered envelope is approximately described by an exponential profile and contains  $L_{V,\text{NE,env}} = 1.2 \times 10^{10} (\pm 6.0 \times 10^8) L_{\odot}$ . This corresponds to  $\sim 50\%$  of the lumi-

nosity of the symmetric halo in the same region, and  $\sim 15\%$  of the luminosity of the entire symmetric halo in the radial range  $23'' - 120''$ .

Furthermore, the diffuse light in the Hydra I core harbors two tidal streams emerging from the dwarf galaxy HCC 026 and the S0 galaxy HCC 007 (see Fig. 13). The total luminosity in the NW part of the HCC 026 stream is  $L_{V,\text{NW,HCC 026}} = 4.8 \times 10^8 (\pm 8 \times 10^7) L_{\odot}$ , with an average surface brightness  $\mu_V = 24.8 \pm 0.2$  mag arcsec<sup>-2</sup>,  $\sim 15\%$  of that in the extended envelope and symmetric halo at the stream position.

Analysis of a deep spectrum in this region indicates that the NW stream has a LOS-velocity similar to HCC 026 itself ( $\sim 5000$  km s<sup>-1</sup>; see Sect. 5), and that it consists of stars with similar metallicities as the stars of HCC 026 (Coccato et al. 2011a). These results favour the interpretation that the HCC 026 stream has been tidally dissolved from HCC 026, over one where both the dwarf galaxy and the stream were dissolved from a larger galaxy. The luminosity of the combined NW and SE parts of the stream is several times the current luminosity of HCC 026,  $L_{V,\text{HCC 026}} = 1.5 \times 10^8 L_{\odot}$ , so that this dwarf galaxy has by now been mostly dissolved by the tidal field. Both HCC 026 and its tidal tails have a relative LOS velocity of  $\sim 1200$  km s<sup>-1</sup> with respect to NGC 3311 ( $V_{\text{NGC3311}} \simeq 3800$  km s<sup>-1</sup>).

The second tidal stream around the S0 galaxy HCC 007 extends over at least  $\sim 110$  kpc on both sides of this galaxy. The tail is fairly thick and is brighter on the NE side where  $\mu_V = 24.4 \pm 0.5$  mag arcsec<sup>-2</sup>, than on the NW side where it is about one magnitude fainter. We measured a luminosity of  $L_{V,\text{NE,HCC 007}} = 2.9 \times 10^9 (\pm 5 \times 10^8) L_{\odot}$  in the brightest region of the NE tail. The NE tail appears to join the outer part of the off-centered halo east of NGC 3311; if so, its total luminosity could be significantly higher. For comparison, the total current luminosity of HCC 007 is  $\sim 4.7 \times 10^9 L_{\odot}$ . This galaxy has therefore lost of order 50% of its stars.

Three PNs are found on the NE HCC 007 tail which allow a preliminary measurement of its LOS velocity. The largest PN velocity ( $5470$  km s<sup>-1</sup>) is found SE of NGC 3311 in a region dominated by tail stars. One PN is close to HCC 007 itself and has a velocity within  $60$  km s<sup>-1</sup> of the galaxy's systemic velocity.

The morphologies of these streams are similar to those of tidal streams generated when galaxies are disrupted on highly radial orbits through the cluster center, shortly after the time of closest approach with the cluster cD (Rudick et al. 2009).

Superposed on the off-centered outer halo of NGC 3311, we also find a number of PNs from the same sub-component of the PN LOSVD centered at  $5000$  km s<sup>-1</sup>, as well as a group of dwarf galaxies with similar velocities. This suggests a physical association between the off-centered halo, the two tidal streams, and an entire group of galaxies at about  $5000$  km s<sup>-1</sup> systemic velocity,

including HCC 026, several other dwarf galaxies, and HCC 007, which are currently falling through the core of the Hydra I cluster and have already been partially disrupted.

What fraction of the off-centered halo is due to stars dissolved from these galaxies is, however, not constrained well by our measurements. The deep spectra show only a modest shift in mean LOS velocity in the NE halo, and the photometric, kinematic and stellar population analysis of the HCC 026 tail suggests that the component at  $5000 \text{ km s}^{-1}$  LOS velocity contributes only a fraction of the inferred off-centered halo at this location. Furthermore, a number of PNs with moderately to highly blue-shifted velocities are also seen superposed on the outer halo of NGC 3311 (Ventimiglia et al. 2011). To resolve this requires further kinematics and stellar population analysis with deep spectroscopy at different positions in the halo.

This work provides a vivid example of how strong tidal forces cause morphological transformations of galaxies falling through the cores of galaxy clusters. It also shows that stars are currently being added to the diffuse light in the Hydra I cluster core. The stars in the streams around HCC 026 and HCC 007 must have been unbound from their parent galaxies during the on-going close passage through the high-density center of the cluster, and are now on slightly different orbits from their once parent galaxies. Ultimately they will phase-mix in the potential and add to the diffuse outer envelope of NGC 3311 and to the intracluster light in the cluster core.

The on-going accretion of a group of galaxies will add about several  $10^9 L_{\odot,V}$  to the outer halo and intracluster light around NGC 3311, about 5% of the total light in the NGC 3311 symmetric halo. Tidal dissolution of small galaxies is thus an important channel for creating diffuse light in clusters. It is unlikely, however, that this is the main mechanism for the origin of the symmetric halo around NGC 3311. Both simulations (Murante et al. 2007; Puchwein et al. 2010) and studies of diffuse light in clusters like Coma and the star pile cluster (Gerhard et al. 2007; Salinas et al. 2011) indicate that the disruption and merger of a giant galaxy is the more efficient route to creating large amounts of diffuse light. Deep spectroscopy to measure Lick indices and stellar abundances in different regions of the offset envelope and halo of NGC 3311 will be important to address this issue further.

*Acknowledgements.* The authors thank the referee for his/her constructive report, the ESO VLT staff for their support during the observations, and Ken Freeman for helpful discussions during the course of this project. They also thank Ricardo Salinas and Tom Richtler for sending their NGC 3311 kinematic data in electronic form. EI acknowledges support from ESO during several visits while this work was completed. LC acknowledges funding from the European Community's Seventh Framework Programme (FP7/2007-2013/) under grant agreement No 229517. This research has made use of the 2MASS data archive and the NASA/IPAC Extragalactic Database (NED), and of the ESO Science Archive Facility.

## References

Arnaboldi, M. & Gerhard, O. 2010, *Highlights of Astronomy*, 15, 97  
 Arnaboldi, M., Gerhard, O., Okamura, S., et al. 2007, *PASJ*, 59, 419  
 Buzzoni, A., Arnaboldi, M., & Corradi, R. L. M. 2006, *MNRAS*, 368, 877  
 Cappellari, M. & Emsellem, E. 2004, *PASP*, 116, 138  
 Ciardullo, R., Jacoby, G. H., Ford, H. C., & Neill, J. D. 1989, *ApJ*, 339, 53  
 Coccato, L., Arnaboldi, M., Gerhard, O., et al. 2010a, *A&A*, 519, A95  
 Coccato, L., Gerhard, O., & Arnaboldi, M. 2010b, *MNRAS*, 407, L26  
 Coccato, L., Gerhard, O., Arnaboldi, M., et al. 2009, *MNRAS*, 394, 1249  
 Coccato, L., Gerhard, O., Arnaboldi, M., & Ventimiglia, G. 2011a, *A&A*, 533, A138  
 Coccato, L., Morelli, L., Corsini, E. M., et al. 2011b, *MNRAS*, 412, L113  
 De Lucia, G. 2007, in *Astronomical Society of the Pacific Conference Series*, Vol. 379, *Cosmic Frontiers*, ed. N. Metcalfe & T. Shanks, 257–  
 Doherty, M., Arnaboldi, M., Das, P., et al. 2009, *A&A*, 502, 771

Dolag, K., Murante, G., & Borgani, S. 2010, *MNRAS*, 405, 1544  
 Faltenbacher, A. & Mathews, W. G. 2005, *MNRAS*, 362, 498  
 Gerhard, O., Arnaboldi, M., Freeman, K. C., et al. 2005, *ApJ*, 621, L93  
 Gerhard, O., Arnaboldi, M., Freeman, K. C., et al. 2007, *A&A*, 468, 815  
 Gonzalez, A. H., Zabludoff, A. I., & Zaritsky, D. 2005, *ApJ*, 618, 195  
 Hayakawa, A., Furusho, T., Yamasaki, N. Y., Ishida, M., & Ohashi, T. 2004, *PASJ*, 56, 743  
 Hayakawa, A., Hoshino, A., Ishida, M., et al. 2006, *PASJ*, 58, 695  
 Jacoby, G. H. 1989, *ApJ*, 339, 39  
 Janowiecki, S., Mihos, J. C., Harding, P., et al. 2010, *ApJ*, 715, 972  
 Jarrett, T. H., Chester, T., Cutri, R., Schneider, S. E., & Huchra, J. P. 2003, *AJ*, 125, 525  
 Kelson, D. D., Zabludoff, A. I., Williams, K. A., et al. 2002, *ApJ*, 576, 720  
 Laine, S., van der Marel, R. P., Lauer, T. R., et al. 2003, *AJ*, 125, 478  
 McNeil, E. K., Arnaboldi, M., Freeman, K. C., et al. 2010, *A&A*, 518, A44+  
 Mendel, J. T., Proctor, R. N., Rasmussen, J., Brough, S., & Forbes, D. A. 2009, *MNRAS*, 396, 2103  
 Mihos, J. C., Harding, P., Feldmeier, J., & Morrison, H. 2005, *ApJ*, 631, L41  
 Misgeld, I., Mieske, S., & Hilker, M. 2008, *A&A*, 486, 697  
 Murante, G., Arnaboldi, M., Gerhard, O., et al. 2004, *ApJ*, 607, L83  
 Murante, G., Giovali, M., Gerhard, O., et al. 2007, *MNRAS*, 377, 2  
 Murphy, J. D., Gebhardt, K., & Adams, J. J. 2011, *ApJ*, 729, 129  
 Napolitano, N. R., Pannella, M., Arnaboldi, M., et al. 2003, *ApJ*, 594, 172  
 Peng, C. Y., Ho, L. C., Impey, C. D., & Rix, H. 2002, *AJ*, 124, 266  
 Poggianti, B. 2004, in *Baryons in Dark Matter Halos*, ed. R. Dettmar, U. Klein, & P. Salucci  
 Puchwein, E., Springel, V., Sijacki, D., & Dolag, K. 2010, *MNRAS*, 406, 936  
 Richtler, T., Salinas, R., Misgeld, I., et al. 2011, *ArXiv e-prints*  
 Rudick, C. S., Mihos, J. C., Frey, L. H., & McBride, C. K. 2009, *ApJ*, 699, 1518  
 Salinas, R., Richtler, T., West, M. J., et al. 2011, *A&A*, 528, A61  
 Sanchez-Blazquez, P., Peletier, R. F., Jimenez-Vicente, J., et al. 2007, *VizieR Online Data Catalog*, 837, 10703  
 Schlegel, D. J., Finkbeiner, D. P., & Davis, M. 1998, *ApJ*, 500, 525  
 Seigar, M. S., Graham, A. W., & Jerjen, H. 2007, *MNRAS*, 378, 1575  
 Sersic, J. L. 1968, *Atlas de galaxies australes*, ed. Sersic, J. L.  
 Sommer-Larsen, J., Romeo, A. D., & Portinari, L. 2005, *MNRAS*, 357, 478  
 Tal, T., van Dokkum, P. G., Nelan, J., & Bezanson, R. 2009, *AJ*, 138, 1417  
 Thuan, T. X. & Kormendy, J. 1977, *PASP*, 89, 466  
 Tonry, J. & Davis, M. 1979, *AJ*, 84, 1511  
 Vasterberg, A. R., Lindblad, P. O., & Jorsater, S. 1991, *A&A*, 247, 335  
 Ventimiglia, G., Arnaboldi, M., & Gerhard, O. 2008, *Astronomische Nachrichten*, 329, 1057  
 Ventimiglia, G., Arnaboldi, M., & Gerhard, O. 2011, *A&A*, 528, A24+  
 Ventimiglia, G., Gerhard, O., Arnaboldi, M., & Coccato, L. 2010, *A&A*, 520, L9+  
 Willman, B., Governato, F., Wadsley, J., & Quinn, T. 2004, *MNRAS*, 355, 159